ACS OMEGA

Open Access



http://pubs.acs.org/journal/acsodf

Review

# A Short Review on the Evolution of Magnetocaloric $La(Fe,Si)_{13}$ and Its Fabrication through Melt Spinning

*Published as part of ACS Omega virtual special issue "Magnetic Nanohybrids for Environmental Applications".*

Anjana Vinod, D. Arvindha Babu, and Madhuri Wuppulluri*

Cite This: *ACS Omega* 2024, 9, 11110−11128

Read Online

ACCESS | Metrics & More | Article Recommendations

**ABSTRACT:** Energy-efficient refrigeration technology needs to advance ineluctably due to rising energy consumption and diminishing fossil fuel and primitive hydrocarbon reserves. Further, the existing gas compression method releases huge amount of chlorofluorocarbons (CFCs) that deplete the ozone layer. This is a global concern, which demands an immediate remedial technology. As a potential solution to the problem of sustainability and a means of meeting the ever-increasing demand for energy, environmentally friendly and socially responsible renewable energy sources could serve as an ideal replacement for traditional refrigeration technology. Solid-state refrigeration using magnetocaloric materials is one prominent technique that can be adopted for clean and economical refrigeration or cooling requirements. In this review, we briefly introduce the present understanding on magnetocaloric $LaFe_{13-x}Si_x$ alloys with a specific emphasis on their application in magnetic refrigeration. This paper deals with the advantages and disadvantages of different synthesis methods for producing $LaFe_{13-x}Si_x$ and enhancing its magnetocaloric effects. Annealing time, yield, composition, and relative cooling power are examined as prospective industrial implementation factors for the $La(Fe,Si)_{13}$ synthesis process. The initial sections have been devoted to an overview of the magnetocaloric effect and its different types and history. Further, the article reviews the evolution of a new preparation method called melt spinning, other synthesizing methods, and some developments around the world for the prototypes of La(Fe,Si)-based magnetic refrigeration methods. According to the findings in the scholarly literature, the synthesis process of melt spinning has the potential to be commercialized because of its capacity to create huge quantities of $La(Fe,Si)_{13}$ with a high purity in a very short amount of time.

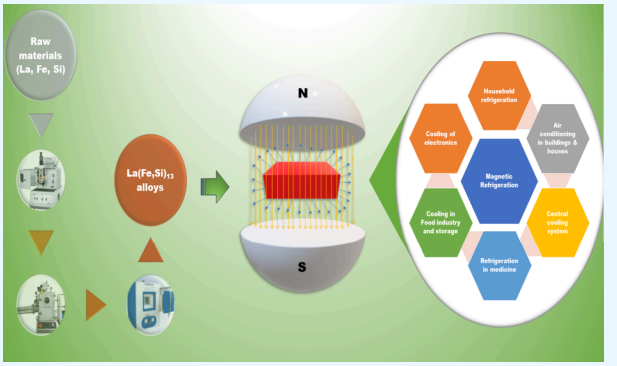


## 1. INTRODUCTION

Enhanced adoption of renewable energy sources as well as increased efficiency in end-use applications are required for a sustainable remedy to the problem of finite fossil fuel resources in the light of rising global energy needs. In affluent nations like the United States, refrigeration uses 7% of all commercial energy and 5% of all residential energy.[1] 61% of the predicted United States (USA) energy consumption in 2015 belongs to unused energy, according to the data from Laurence Livermore National Laboratory, while only 39% is really engaged in energy service.[2] These findings show that, in addition to concentrating on our major sources of energy and reducing our reliance on energy sources that are not renewable, significant research efforts must also be made to increase the effectiveness of energy conversion.[3]

The destruction of the ozone layer is the main environmental problem we are experiencing nowadays.[4] No effective way to reduce the number of greenhouse gases released into the atmosphere by human activity has been discovered, despite the adoption of many protocols such as those of Kyoto and Montreal. Conventional vapor compression refrigeration uses chemicals as refrigerants, which have the potential to drain into the environment and cause ozone layer depletion and greenhouse effect augmentation.[5]

The magnetocaloric effect (MCE) at room temperature allows for magnetic refrigeration to be used as an alternative to traditional cooling methods.[6] Great refrigeration efficiency, dependability, low noise, and environmental friendliness are some of the advantages of this method.[7] Various applications of magnetic refrigeration in different areas are showed in

Received: October 31, 2023
Revised: January 18, 2024
Accepted: January 30, 2024
Published: February 27, 2024

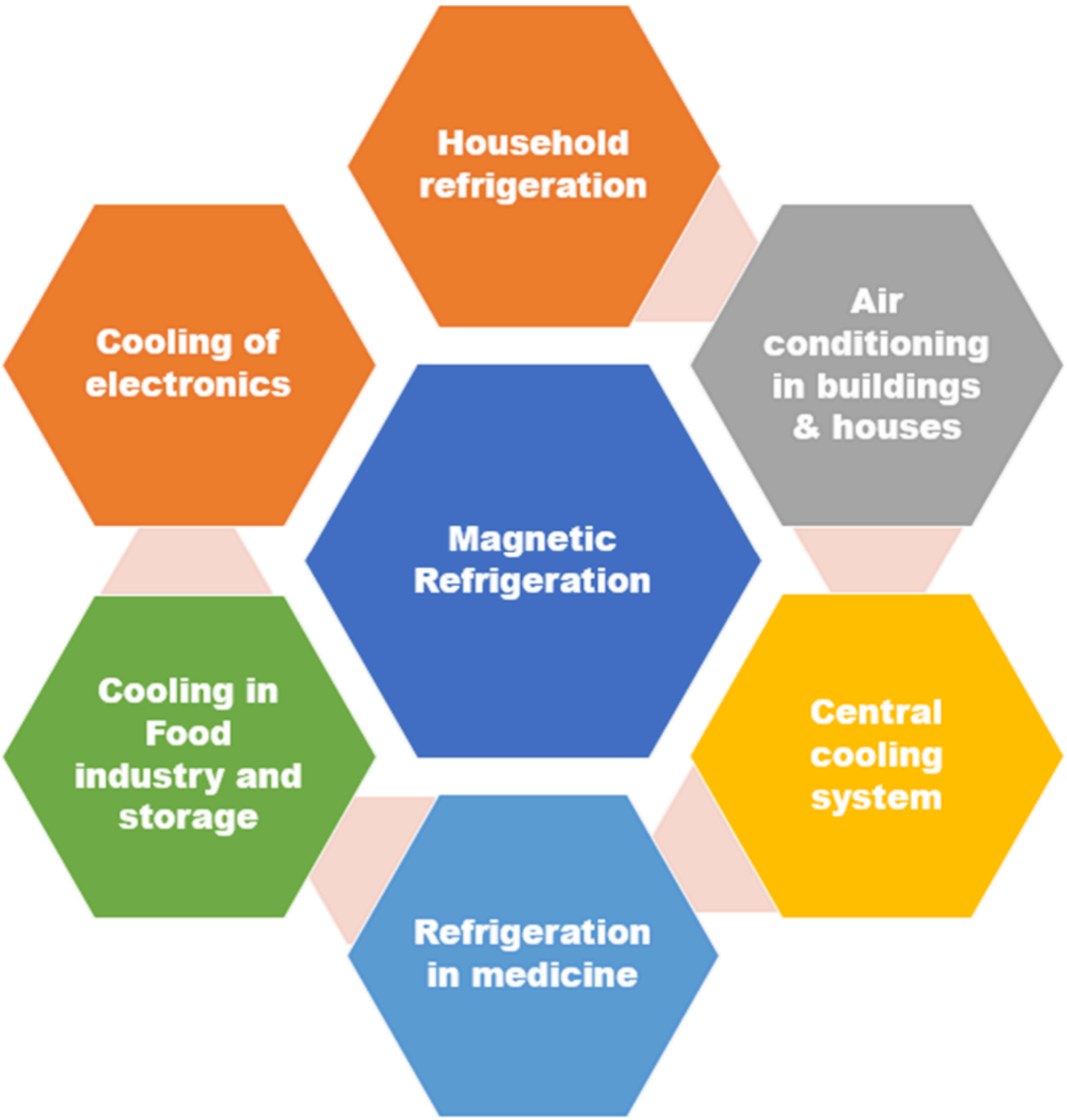


**Figure 1.** Various magnetic refrigeration applications in different areas.

Figure 1. Emil Warburg first observed the MCE in iron (Fe), which is a critical component of magnetic materials.[5] This phenomenon can be used to the benefit of a variety of magnetocaloric devices, including magnetic energy converters, magnetic heat pumps, and magnetic refrigerators.[8]

Due to its many benefits over traditional gas compression refrigeration, including its high efficiency, low energy consumption, and low impact on the environment, the relatively new field of room-temperature magnetic refrigeration has garnered a lot of interest as a promising new refrigeration technology.[9,10] Other magnetic refrigeration materials, such as $Gd_5(Si_xGe_{1-x})_4$, $MnAs_{1-x}Sb_x$, $La(Fe_{1-x}Si_x)_{13}$, and $MnFeP_{1-x}As_x$, are already commercially available.[11] Fe-based compounds with cubic $NaZn_{13}$ type structures have been presented as excellent materials for exploring efficient magnetic refrigerants due to their high magnetization, good soft ferromagnetism, and inexpensive cost. These characteristics make them ideal candidates for this line of research.[12] $La(Fe,Si)_{13}$ phases (with a cubic $NaZn_{13}$ structure) have a significant magnetocaloric impact when combined with a first-order phase transition.[2] $La(Fe_{1-x}Si_x)_{13}$ compounds of the $NaZn_{13}$ type[10] have attracted a lot of attention in research because of their high MCE, low cost, and flexible operating temperature.[13] In this overview, an attempt has been made to review the present understanding of $NaZn_{13}$-type $La(Fe_{1-x}Si_x)_{13}$ compounds for magnetocaloric refrigeration applications followed by different synthesis methods, and mainly melt spinning is highlighted.


https://doi.org/10.1021/acsomega.3c08622
ACS Omega 2024, 9, 11110−11128

## 2. HEUSLER ALLOYS

Although magnetism has piqued man's interest, our knowledge of the phenomenon is very new and still insufficient. Almost all naturally existing magnetic minerals contain the element iron, and all artificial magnetic materials up until the 20th century were made of at least one of the ferromagnetic transition metals, such as iron, cobalt, or nickel. Friedrich Heusler, a German chemist and mining engineer, found that the Cu-Mn-Al alloy is ferromagnetic material despite of the fact that it contains nonferromagnetic components, demonstrating that ferromagnetic alloys may be made entirely of nonferromagnetic elements.[14] Heusler alloys are intermetallic compounds having magnetic characteristics that may be changed by varying the chemical order, degree, or type.[15]

Heusler alloys are divided into five categories which are shown in Figure 2. They are

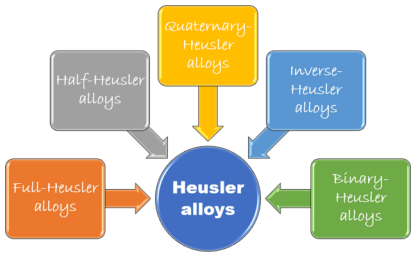


**Figure 2.** Classification of Heusler alloys.

(1) full-Heusler alloys ($X_2YZ$)
(2) half-Heusler alloys (XYZ)
(3) quaternary Heusler alloys ($XX^1YZ$)
(4) inverse Heusler alloys ($X_2YZ$)
(5) binary Heusler alloys ($X_3Z$)[5]

where Z is an element from the periodic table's III−V group and X and Y are elements from the transition metal group.[16]

Different types of Heusler alloys with general formula, crystal structure, Wyckoff structure, space group, and examples of each are given in Table 1. Crystal structures of full-Heusler alloys are composed of four interpenetrating fcc sublattices, of which two are completely and uniformly filled with X.[20] As these two X-site fcc sublattices unite to create a simple cubic lattice, the Y and Z atoms alternately inhabit the simple cubic lattice's centers.[21] These are powerful ferromagnets with a magnetic moment of up to 7 $\mu_B$ and a high Curie transition temperature of 600 K as in $Co_2MnSi$, $Co_2MnGe$, ... Half-Heusler alloys are expected to be ferromagnetic with a high Curie transition temperature of 500−700 K,[22] and some of the compounds with iron (Fe) and rhodium (Rh) have a Curie transition temperature at about room temperature.[22] Half-Heusler alloys, such as NiMnSb and TiNiSn, have the chemical formula XYZ (1:1:1). These compounds, according to Graf et al.,[7] have ionic and covalent components, with X and Y elements having cationic character and Z having an anionic component. The main-group atom Z interacts with the most electropositive element X to form a rock-salt (NaCl) sublattice, and this contact strengthens the ionic nature of their bonding. Covalent bonding is indicated by the zinc-blende (ZnS) sublattice that is formed by the Y and Z atoms as shown in Figure 9.[23] As a result, the structure of half-Heusler alloys is composed of lattices made of zinc blende (ZnS) and sodium chloride (NaCl).[4] The maximum magnetic moment of these half-Heusler alloys is 5 $\mu_B$. $C1_b$ crystal structures distinguish-half-Heusler alloys from full-Heusler alloys which exhibit $L2_1$ crystal structures.[4]

The inverse-Heusler alloys are other types of Heusler alloys that is obtained from full-Heusler alloys. Consequently, they adhere to the identical chemical composition $X_2YZ$. Though they descended from full-Heusler alloys, inverse-Heusler alloys crystallize in the XA or X$\alpha$ structure with $F4_3m$ symmetry. The X elements in these alloys do not display a straightforward cubic configuration, but they do have four interpenetrating fcc sublattices. Some inverse-Heusler alloys are $Hg_2TiCu$, $Zr_2PdAl$, etc.[24]

Quaternary-Heusler alloys (QHAs) with 4d and 4f electrons are the least studied of the aforementioned varieties in the Heusler alloy family. The QHAs have the chemical formula XX′YZ. But instead of being generated by a single element, X and X′ are made up of many transition group elements. Another feature of these alloys is that X atoms have a higher valence than X′, while Y atoms have a lower valence than both X and X′ elements. CoFeCrAs, CoMnVAs, CoFeCrZ (Z = Si, As, Sb), and CoFeCrX (X = Si, Ge) are a few of the theoretically and empirically synthesized QHAs. They have a high Curie transition temperature and a high thermoelectric efficiency, and they are semimetallic alloys.[17]

The chemical composition of binary-Heusler alloys is represented by the formula $X_3Z$ (3:1), where X denotes transition metal elements and Z represents the main group elements. These alloys have a face-centered-cubic (fcc) $D0_3$-type crystal structure and have the space group of $Fm3m$.[17]

Half metallic behavior, inverse magnetocaloric effect, and magnetic shape memory effect[25] are three distinctive features of Heusler alloys that have recently piqued experimental and theoretical attention. Any substance that behaves as a conductor to electrons with a certain spin orientation but as

**Table 1. Classification of Heusler Alloys and Their Properties**

| type of Heusler alloy | general formula | crystal structure | space group | Wycoff position | example |
|---|---|---|---|---|---|
| full-Heusler alloys | $X_2YZ$ | $L2_1$ | $Fm3m$ | 8c $\left(\frac{1}{4},\frac{1}{4},\frac{1}{4}\right)$, 4b $\left(\frac{1}{2},\frac{1}{2},\frac{1}{2}\right)$, 4a (0,0,0) | $Cu_2MnSn$, $Cu_2MnAl$, $Co_2MnGe$, $Co_2MnSi$[17] |
| half-Heusler alloys | XYZ | $C1_b$ | $F43m$ | 4b $\left(\frac{1}{2},\frac{1}{2},\frac{1}{2}\right)$, 4c $\left(\frac{1}{4},\frac{1}{4},\frac{1}{4}\right)$, 4a (0,0,0) | NiMnSb, TiNiSn[17,18] |
| quaternary-Heusler alloys | XX′YZ | | $F4_3m$ | 4a (0,0,0), 4b $\left(\frac{1}{2},\frac{1}{2},\frac{1}{2}\right)$, 4c $\left(\frac{1}{4},\frac{1}{4},\frac{1}{4}\right)$, 4d $\left(\frac{3}{4},\frac{3}{4},\frac{3}{4}\right)$ | LiMgPdSn, CoFeMnSi[17,19] |
| inverse-Heusler alloys | $X_2YZ$ | | $F4_3m$ | 4a (0,0,0), 4c $\left(\left(\frac{1}{4},\frac{1}{4},\frac{1}{4}\right)\right.$, 4b $\left(\frac{1}{2},\frac{1}{2},\frac{1}{2}\right)$, 4d $\left(\frac{3}{4},\frac{3}{4},\frac{3}{4}\right)$ | $Hg_2TiCu$, $Zr_2PdAl$[17] |
| binary-Heusler alloys | $X_3Z$ | $D0_3$ | $Fm3m$ | $\left(\frac{1}{4},\frac{1}{4},\frac{1}{4}\right)$ for X(A), $\left(\frac{3}{4},\frac{3}{4},\frac{3}{4}\right)$ for X(C), $\left(\frac{1}{2},\frac{1}{2},\frac{1}{2}\right)$ for X(B), (0,0,0) for Z | $LiO_3$, $NaN_3$, $BeCl_3$[17] |



https://doi.org/10.1021/acsomega.3c08622
ACS Omega 2024, 9, 11110−11128

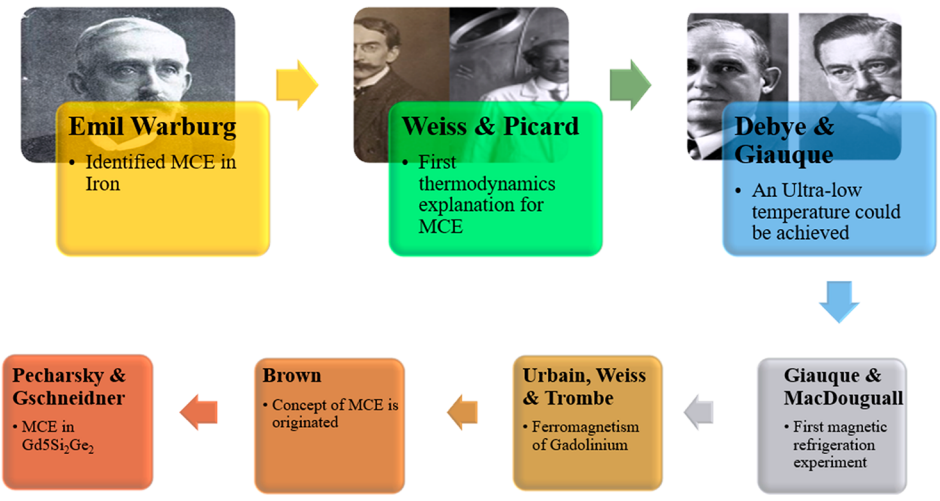


**Figure 3.** Timeline of the history of magneto caloric effect. Reproduced with permission from refs 34−38. Copyright public domain.

an insulator or semiconductor to electrons with an opposite spin orientation is referred to as a half metal.[26] One of the examples of this type of material is NiMnSb. The term "magnetic shape memory" refers to a magnetic material's ability to alter shape or size when subjected to a magnetic field. Examples are $Ni_2MnGa$ and $Co_2NbSn$. In $Ni_2MnSn$ and NiMnSn Heusler alloys inverse MCE has been reported.[5] The inverse magnetocaloric effect of Heusler alloys refers to the adiabatic cooling of the sample by the application of a magnetic field.[27,4] This property is thought to be promising for the creation of a cost-effective and environmentally friendly refrigerant that operates at or near room temperature.[3] This property is viewed as promising for the creation of a reasonably priced and environmentally friendly refrigerant that functions at or near room temperatures.

## 3. A BRIEF HISTORY OF MCE

Figure 3. depicts the timeline of history of the magnetocaloric effect. As mentioned previously, Emil Warburg first identified MCE on iron (Fe) in 1881. He made several observations in this area and discovered that the rise in temperature observed in iron wires is due to a magnetization and demagnetization cycle.[28] The following were his experimental conditions.

(1) His experiment used a magnetic field that was 100 times stronger than the magnetic field of the earth's magnetic field in Freiburg.[28]
(2) He conducted his studies at room temperature.[28]
(3) He did not take any direct or indirect readings; instead, he made an approximation based on the area of the hysteresis loop that the iron wire displayed when it was magnetized and demagnetized which was converted into a temperature difference in the corresponding temperature change in water's quantity.[28]
(4) Due to the reversible nature of the magnetocaloric effect in iron and the fact that both magnetization and demagnetization were a part of Warburg's cycle, the resulting magnetocaloric temperature was zero.[28]

Weiss and Piccard presented the first thermodynamic explanation for the magnetocaloric effect in 1917. They discovered that in nickel (Ni), a temperature change of 0.7 K with a magnetic field of 1.5 T is measured at the Curie transition temperature, which is at 598 K.[28,17] As a result, they were able to identify the rather standard magnetocaloric effect's distinguishing features: specifically that it is reversible and secondly that its maximum temperature change is close to the Curie transition temperature.[28]

Debye and Giauque were the first to recognize the technological potential of this phenomena during their independent studies from 1926 to 1927 that an ultralow temperature could be achieved by reversibly changing the temperature of paramagnetic (PM) compounds with an alternating magnetic field. Giauque also won the Nobel Prize in 1949 for his discovery.[29] Giaugue and MacDougall carried out the first magnetic refrigeration experiment in 1933, successfully achieving temperatures below 1 K with the use of the technology.[2]

Prior to the discovery of gadolinium's ferromagnetism by Urbain, Weiss, and Trombe in 1935, no ferromagnetic substance with a Curie transition point near room temperature was known. An exceptional paper by Brown from 1976 is when the concept of magnetocaloric effect based near-room-temperature magnetic refrigeration originated.[30] In 1997, Pecharsky and Gschneidner made the crucial discovery that would forever change the field of materials science: the enormous magnetocaloric phenomena in $Gd_5Si_2Ge_2$. They discovered a magnetocaloric effect at a first-order transition between two distinct ferromagnetic phases at 276 K that was greater than that of any other known magnetic material, including gadolinium.[28]

A massive MCE in MnFe(P,As) alloys was demonstrated in 2002 by a team of researchers from the University of Amsterdam in The Netherlands. Since then, many designs and types of magnetic refrigeration systems as well as novel magnetocaloric materials have been created.[31] Although magnetic refrigeration is a promising technique, there are still many obstacles to overcome, including finding appropriate materials with strong magnetocaloric characteristics.[32] Therefore, research into novel materials with strong magnetocaloric characteristics is necessary for real-world applications at subroom and room temperatures.[33]

## 4. MAGNETOCALORIC EFFECT

The magnetocaloric effect (MCE) based magnetic refrigeration has developed as a potential alternative technology for traditional refrigeration systems in recent years.[39,40] Replacing conventional compression or expansion systems by magneto-


https://doi.org/10.1021/acsomega.3c08622
ACS Omega 2024, 9, 11110−11128

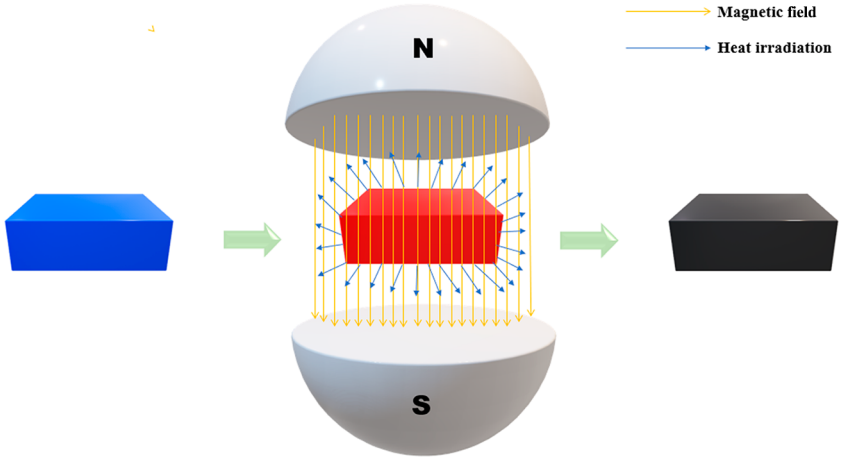


**Figure 4.** Schematic illustration of the magnetocaloric effect.

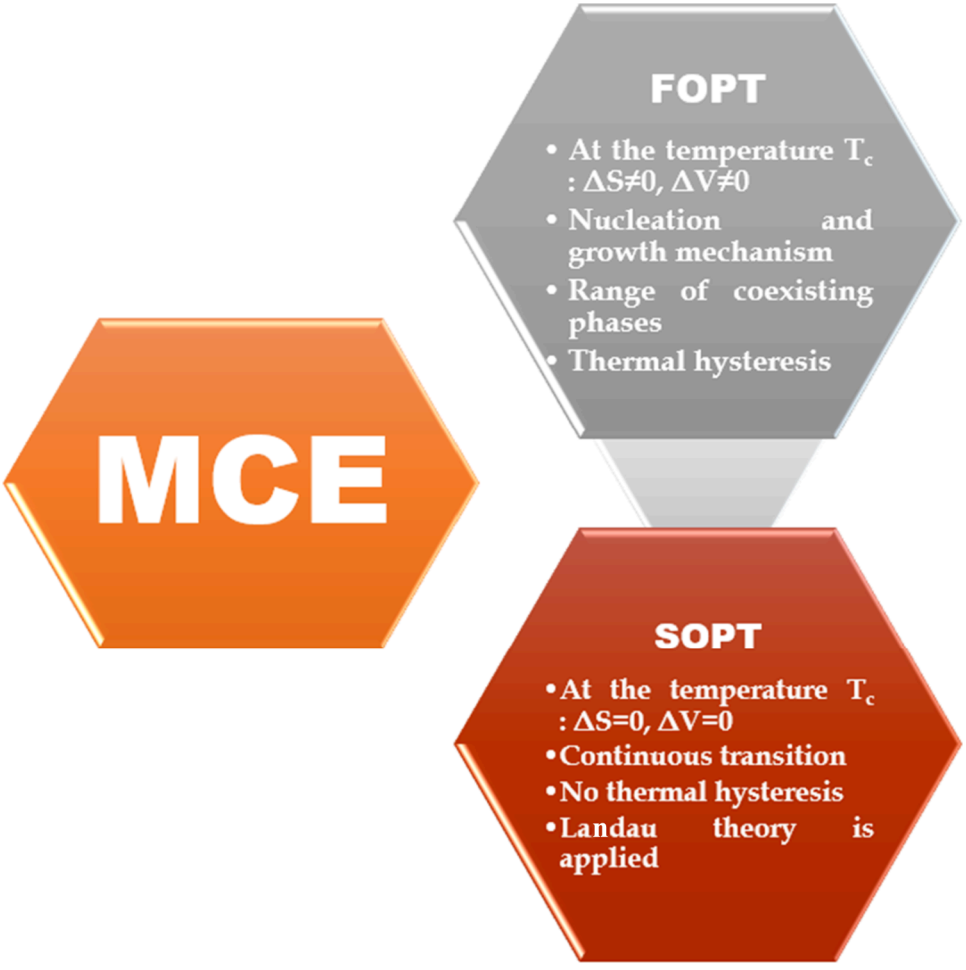


**Figure 5.** Different types of magnetocaloric effects.

caloric materials provides an energy efficiency increase of up to 30%, more compact systems, minimal noise, and no emission of gaseous pollutants.[13] MCE not only eliminates the use of harmful chemicals (ammonia), ozone-depleting substances (CFCs), greenhouse gases (hydrochlorofluorocarbons), and ozone-depleting substances (HCFCs) but it also has the potential to cut world energy consumption.[41] This technology offers a number of benefits, including great durability, low noise, and environmental friendliness.[42] Several magnetocaloric devices, such as magnetic energy conversion devices, magnetic heat pumps, and magnetic refrigerators, can utilize this phenomenon.[5]

Due to their capacity for thermal energy exchange with the environment, magnetic materials[43] can generate heat when they are in a magnetic field by aligning their magnetic moments.[13] The magnetic materials became colder than the atmosphere when the magnetic field was eliminated,[44] which is schematically shown in Figure 4. The heat produced as a result


https://doi.org/10.1021/acsomega.3c08622
ACS Omega 2024, 9, 11110−11128

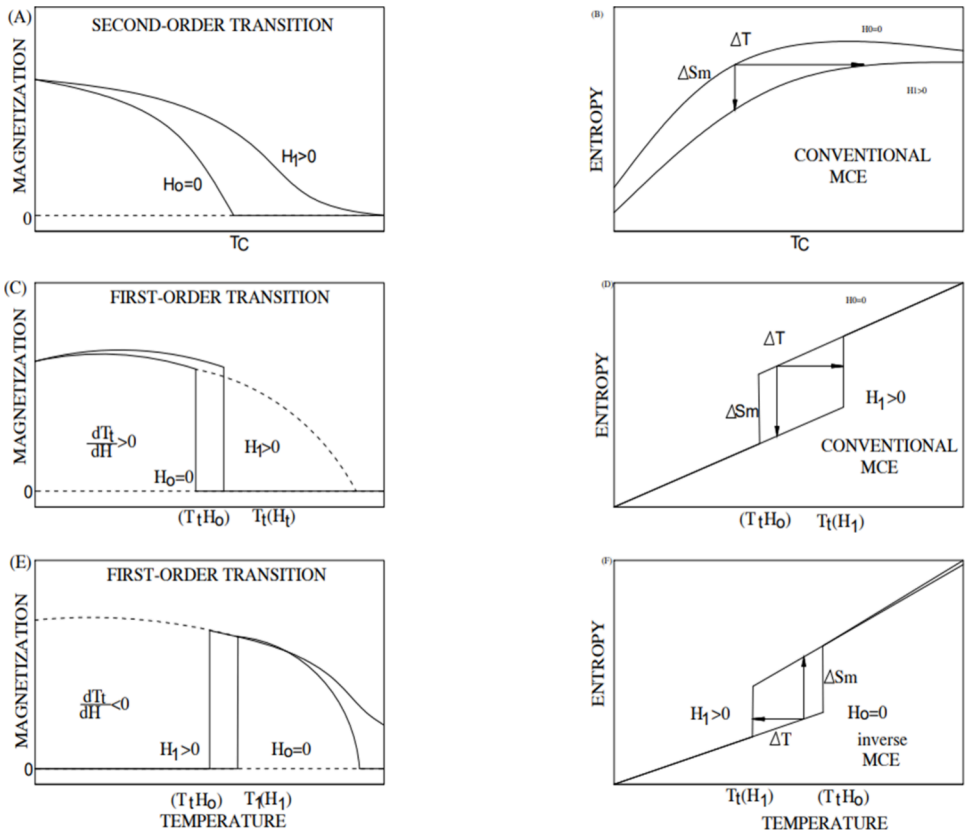


**Figure 6.** Schematic illustration of difference between the first-order phase transition (FOPT) and second-order phase transition (SOPT). Reprinted with permission from ref 53. Copyright 2016, Royal Society of Chemistry.

of this process can be converted to electricity by reversing the process.[43]

The MCE is characterized by a significant isothermal entropy shift ($\Delta S_M$) and an adiabatic temperature change ($\Delta T_{ad}$).[45] The refrigerant capacity (RC), in addition to the $\Delta S_M$, is a recognized criterion for determining refrigeration efficiency. The magnetization and heat capacity can be determined experimentally and used to calculate the MCE ($\Delta S_M$ and $T_{ad}$) directly or indirectly. An increase in the applied field causes a decrease in magnetic entropies and an increase in the rate at which heat is transmitted from the system into the environment via an isothermal process; on the other hand, when there is a reduction in the amount of magnetic field that is being applied, magnetic entropies will increase, and there will be a transfer of heat from the lattice system into the magnetic system via an adiabatic process.[46]

Numerous materials have been thoroughly investigated for magnetic refrigeration at low temperatures, such as the intermetallic compound of rare earth elements (RE = Eu, Gd, Ho, Er, Tm) with low-boiling-point metals (Zn, Cd, and Mg), $RE_2T_2X$ (RE = Gd−Tm; T = Ni, Co, Cu; X= Ga, Al, Sn, Cd, In),[47] $Tm_{60}Co_{20}Ni_{20}$, $RE_{55}Ni_{18}Al_{27}$, etc. The heat transported by each magnetization−demagnetization cycle of the refrigerator should be quite large to ensure refrigeration efficiency. This is due to the high rise in heat capacity near ambient temperature. As a consequence of this, the majority of materials that function at low temperatures are unable to be employed directly;[2] instead, research must be conducted into novel materials that have a significant entropy change at ambient temperature.[48]

Rare earth alloys are the best materials for bringing the Curie transition temperature closer to room temperature.[13] Magnetocaloric materials exhibit a high magnetic entropy change ($\Delta S_M$) in the neighborhood of the Curie transition temperature (and adiabatic temperature change).[49] This occurs as a result of the large magnetic moments and strong magnetization dependence that these alloys exhibit at ambient temperature.[12] Due to their high magnetization, outstanding soft ferromagnetism, and affordable price, Fe-based compounds with cubic $NaZn_{13}$ type structures have been recommended as suitable materials for investigating effective magnetic refrigeration. $La(Fe,Si)_{13}$ with a $NaZn_{13}$ structure[13] has a significant MCE when combined with a first-order phase transition.[2]

**4.1. Classification of MCE.** Based on their physical characteristics, magnetocaloric materials may be divided into several different groups, which are shown in Figure 5. When a material is magnetized, its temperature rises, and when it is demagnetized, its temperature falls; this is the conventional magnetocaloric effect, and it explains why the equivalent change in isothermal entropy is negative (positive) during magnetization (demagnetization).

A first-order phase transition (FOPT) and second-order phase transition (SOPT) are the two types of phase transitions that magnetocaloric materials go through, which is illustrated in Figure 6.[50] First-order material magnetization abruptly shifts at a specific temperature, and latent heat is produced during the phase transition.

Second-order materials show a typical second-order ferromagnetism to paramagnetic transition at a temperature $T_c$, which is shown by the fact that the intrinsic spontaneous magnetization constantly decreases as the temperature rises


https://doi.org/10.1021/acsomega.3c08622
ACS Omega 2024, 9, 11110−11128

toward $T_c$.[28] The benefits of a high magnetic entropy change and adiabatic temperature change in FOPT materials outweigh their disadvantages of thermal hysteresis and poor cycle performance.[51] Although SOPT materials do not experience thermal hysteresis, they have lesser magnetocaloric responses than the majority of FOPT materials operating in the same temperature range.[52]

**4.2. Thermodynamic Cycle in MCE.** MCE is a characteristic that magnetic materials have by origin.[54] Adiabatic magnetization, isothermal enthalpy transfer, adiabatic magnetization, and isothermal entropy transfer are the four steps that comprise the magnetocaloric effect's thermodynamic cycle, which is shown in Figure 7.[8] When a magnetic field is applied

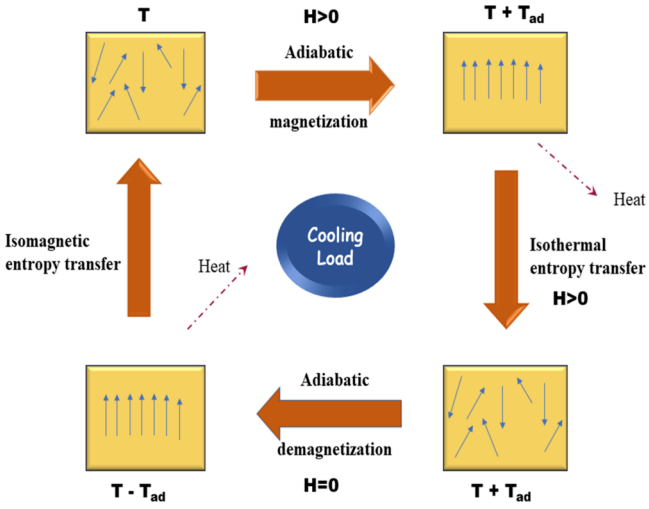


**Figure 7.** Schematic diagram of thermodynamic cycle in MCE.

to a magnetic material, the magnetic dipoles align, the entropy is reduced to $S_M - \Delta S_M$ from $S_M$, the material's temperature is raised to $T + T_{ad}$ from $T$, and the magnetic material's temperature changes adiabatically in the first stage, known as adiabatic magnetization. To stop the magnetic dipoles from reabsorbing the heat by an isothermal enthalpy transfer, the magnetic field is maintained constant. When the externally applied magnetic field is withdrawn during the adiabatic demagnetization process, the magnetic dipoles are no longer aligned and are oriented in a random fashion instead.[55,9] As a result, the temperature drops to $T - T_{ad}$ while the entropy rises to $S_M + \Delta S_M$. When magnetic material is brought in thermal contact with the environment, the environment removes the lowered temperature through isomagnetic entropy transfer, cooling the substance. In order to keep the material from overheating again, the magnetic field is kept constant. The cycle continues until the refrigerant and the chilled surroundings have reached thermal equilibrium.

## 5. Gd-BASED MATERIALS

For a very long time, magnetic refrigeration systems that worked at or near room temperature relied on gadolinium (Gd) in its purest form as the standard working material.[56] It is widely used as a second-order transition material for magnetic refrigeration at low temperatures. With Gd, magnetic refrigerators have been proven to achieve cooling efficiencies of up to 60% of the theoretical limit, whereas the best vapor compression refrigerator achieves just around 40% efficiency. To cool at room temperature with a magnetic field of 2 T or less, which may be created by permanent magnets or electromagnets, researchers are working on producing acceptable Gd-based second-order transition magnetic refrigerants.[41]

In the past, a wide variety of binary alloys based on Gd were studied. $T_c$ and $-\Delta S_M$ are both reduced when Gd is alloyed with rare earth elements including Dy, Ho, Yb, and Tb. Modifications to the Curie transition temperature ($T_c$) caused by the incorporation of transition metals (T) are rather variable.[57] Gd−Mn and Gd−V and Gd−Y alloys have high refrigerative capacity and relative cooling power as compared to Gd, $T_c$ is lowered when T = Mn, V, Co, Ag, Zn, and Y, and $-\Delta S_M$ is decreased rapidly for solidified Gd−Ag alloys and normally in melts of Gd−Zn alloys. As a result of hydrogenation,[58] Gd ($GdH_x$) exhibits improved $T_c$ and $-\Delta S_M$. $-\Delta S_M$ in Gd−X (X = boron, carbon) alloys is found to decrease following alloying Gd, according to the literature.[41] Since Gd's rarity and high price prevent it from being widely used in commercial applications, the quest for an economically cost-effective alternative, lighter rare earth and non rare earth minerals, has begun.[56,59]

## 6. $La(Fe,Si)_{13}$

Gd metal was once thought to be the most promising candidate material, for its near-room-temperature magnetocaloric effect, but its expensive price prompted a shift toward the quest for rare earth elements. Since then, effective magnetic refrigerators have been developed that are cheap, environmentally benign, and capable of operating in wider temperature ranges, which is depicted in Figure 8.[24] $LaFe_{13-x}Si_x$

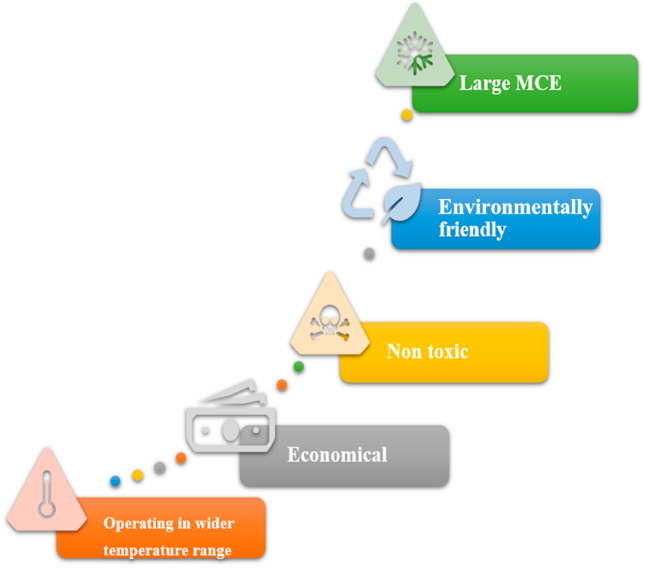


**Figure 8.** Schematic representation of the advantages of $La(Fe,Si)_{13}$ over other magnetocaloric materials.

compounds with a cubic $NaZn_{13}$-type structure have been of interest since the discovery of their large magnetocaloric effect at a cheap cost.[6] These materials can be synthesized without using ultrapure or expensive starting materials, unlike the more popular $Gd(Si,Ge)_4$ combinations.[60] Due to the high Fe component, $La(Fe,Si)_{13}$ type alloys are more promising and cheaper than pure Gd.[4] $LaFe_{13-x}Si_x$ has a thermal conductivity and is orders of magnitude greater than that of $Gd_5(Si,Ge)_4$ and MnAs.[12]


https://doi.org/10.1021/acsomega.3c08622
ACS Omega 2024, 9, 11110−11128

The formation enthalpy of the binary $LaCo_{13}$ phase (−6.31 kJ/mol) is projected to be significantly lower than that of the binary $LaFe_{13}$ phase (1.82 kJ/mol) based on Miedema's model.[61] Due to the positive enthalpy of mixing between the elemental components, $LaFe_{13}$ does not occur naturally. Adding a third ingredient is required to generate $LaFe_{13}$ based alloy. In 1968, Kripyakevich et al. successfully replaced some of the Fe with Si or Al to create the first stable $LaFe_{13-x}M_x$ combination.[2] However, the development of the pseudo binary $La(Fe,Si)_{13}$ phase is improved by adding a tiny amount of Si (10 atom %), which reduces the total free energy of the alloy. At the Curie transition temperature of 195 K, the magnetic entropy change recorded for these alloys can reach up to 31 J/(kg K).[49]

The cubic $NaZn_{13}$ phase structure serves as the basis for the crystal structure of the $La(Fe,Si)_{13}$ type phase (space group *Fm*3*c*).[49] There are 45 different conceivable pairings of rare earth elements with iron, cobalt, or nickel, but only one binary compound, $LaCo_{13}$. The structure of $NaZn_{13}$ reveals two separate Zn sites (Zn I and Zn II). The Na atoms in position 8a and the Zn I atoms in position 8b combine to produce a straightforward CsCl structure. Each Zn I atom at the 96i position has 12 Zn II atoms surrounding it in an icosahedral shape.[22] To be more specific, La takes up residence at the 8a site, Fe fills the entire 8b site, and Si and Fe share the 96i site in $La(Fe,Si)_{13}$ which is shown in Figure 9.[22,24]

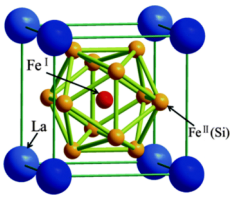


**Figure 9.** Crystal structure of $La(Fe,Si)_{13}$. Reprinted with permission from ref 75. Copyright 2015, Royal Society of Chemistry.

The 1:13 phase formation process and practical preparation techniques are prioritized to ensure the use of $La(Fe,Si)_{13}$ compounds.[62,63] Dual-phase $LaFe_{13-x}Si_x$ alloys often form in the following ways.[64]

(1) The formation of the prime phase $\alpha$-Fe takes place initially.
(2) Peritectic reactions and transformations coarsen the $\alpha$-Fe phase and generate the $La(Fe,Si)_{13}$ phase. The remaining liquid chemical components will approach $La(Fe,Si)_{13}$.
(3) The remainder of the liquid will instantly freeze into the $La(Fe,Si)_{13}$ phase.[64]

According to the La−Fe quasi binary diagram, the peritectic reaction in $LaFe_{13-x}Si_x$ compounds occurs quickly at annealing temperatures between 1407 and 1530 K, with the optimal temperature being 1523 K.[65] The elemental ratio of 1:13 affects magnetic performance as MCE is induced by the 1:13 phase in $LaFe_{13-x}Si_x$ alloys. The melting point of the $La(Fe,Si)_{13}$ phase and peritectoid reaction are 1407.06 and 1530.5 K, respectively. Due to the coupling between the field-induced paramagnetic (PM)−ferromagnetic (FM) transition and discontinuous lattice constant, $LaFe_{13-x}Si_x$ alloys with a cubic $NaZn_{13}$ structure have intriguing physical features including a giant magnetocaloric effect (GMCE).[66]

There are various techniques for the preparation of $LaFe_{13-x}Si_x$ compounds such as arc-melting, induction melting, ball milling, melt spinning, hot pressing, spark plasma sintering, etc.[67] The mixing of rare earth materials to achieve the near-room-temperature Curie transition temperature is the main challenge during the preparation of $LaFe_{13-x}Si_x$.[64]

Ball milling is one technique that may be used to decrease the particle size of bulk materials;[68] however, it is a batch process that makes use of surfactants, which can inhibit magnetic response. Reducing the amount of interfacial pollutants can be accomplished by the use of processes like flame pyrolysis and laser ablation.[13] Flame pyrolysis always results in the production of oxides, which stops the essential phase shift and lowers magnetization. On the other hand, laser ablation is an expensive technique,[3] and it has little potential for being scaled up. The process of changing bulk materials into NPs with the highest purity and practically unlimited material combinations may be accomplished using high-frequency spark ablation, which is an approach that is both straightforward and efficient.[13] In order to make significant strides in both the expansion of our scientific knowledge and the creation of certain useful applications, one of our primary objectives is to investigate feasible and safe substitutes for the production of rare-earth-based magnetic metal alloys on a large scale. The $La(Fe,Si)_{13}$ alloy composition formed by arc melting is compared and detailed in the Table 2. According to Table 2, the magnetic field strength that is applied during the measurement of the change in magnetic entropy[69] is exactly proportional to each other.[70] The data that are presented in Table 2. makes it abundantly evident that the Curie temperature as well as the magnetic characteristics are dependent on the annealing duration as well as the annealing temperature that is chosen in conjunction with the alloy composition.[71] The Curie transition temperature vs change in entropy and temperature vs relative cooling power of various $La(Fe,Si)_{13}$-based materials and different magnetocaloric materials are depicted in Figures 10. and 11, respectively.

Magnetic refrigeration, which is based on the magnetocaloric effect (MCE),[72] shows a lot of potential for competing with the conventional vapor-compression cooling method in terms of being an ecologically friendly and energy-efficient cooling technique. However, the utilization of this category of alloys in certain settings has a number of challenges that must be overcome.[73] It is difficult to acquire directly from ordinary solidification processes[74]

$$\gamma\text{-Fe} + \text{La} \rightarrow \text{La(Fe, Si)}_{13}(\tau_{1a}) \quad (1)$$

which frequently leads in a mixed microstructure of[74]

$$\alpha\text{-Fe} + \text{La(Fe, Si)}_{13}(\tau_{1a}) + \text{LaFeSi}(\tau_4) \quad (2)$$

where the $NaZn_{13}$-type structure in the pseudobinary $LaFe_{13-x}Si_x$ compounds is metastable around ambient temperature. This is because of the intrinsic incompleteness of a peritectic reaction.[65]

$La(Fe,Si)_{13}$ must be prepared in an inert environment due to lanthanum's high atmospheric reactivity. Lanthanum will oxidize and transform into lanthanum oxide when it is exposed directly to the atmosphere. Therefore, a glovebox is necessary during the initial preparation stages, and the sample should be enclosed in a quartz tube before annealing. By creating $LaFe_{13-x}Si_x$ using induction melting or high-vacuum arc melting, we can prevent lanthanum from oxidizing. To obtain single-phase $LaFe_{13-x}Si_x$, it is crucial to consider the chemical


https://doi.org/10.1021/acsomega.3c08622
ACS Omega 2024, 9, 11110−11128

Table 2. Role of Annealing Time and Annealing Temperature on Curie Transition Temperature, Change in Entropy, and Relative Cooling Power of Different Compositions of $LaFe_{13-x}Si_x$ via Arc-Melting Method

| composition | synthesis method | annealing temp (K) | annealing time (h) | $T_c$ (K) | $\Delta S$ (J/(kg K)) | RCP (J/kg) | ref |
|---|---|---|---|---|---|---|---|
| $La_2Fe_{11.0}Si_{2.0}$ | arc-melting | 1423 | 24 | 199 | 14.5 | | 6 |
| $LaFe_{11.0}Si_{2.0}$ | | | | 221 | 7.9 | | 2 |
| $La_2Fe_{11.0}Si_{2.0}$ | arc-melting | | | | 1.5 | 162 | 90 |
| $LaFe_{11.2}Si_{1.8}$ | | | | 210 | 13.0 | | 2 |
| $LaFe_{11.3}Si_{1.7}$ | arc-melting | 1373 | 360 | | 32.6 | 439 | 5 |
| $LaFe_{11.3}Si_{1.7}$ | arc-melting | 1423 | 720.5 | 228.5 | 32.6 | 439 | 24 |
| $LaFe_{11.3}Si_{1.7}$ | | | | 206 | 17.6 | | 2 |
| $LaFe_{11.44}Si_{1.56}$ | arc-melting | 1523 | | | | | 4 |
| $LaFe_{11.4}Si_{1.6}$ | | | | 199 | 18.7 | | 2 |
| $LaFe_{11.4}Si_{1.6}$ | arc-melting | 1273 | 720 | 209 | 19.3 | | 2 |
| $LaFe_{11.4}Si_{1.6}$ | arc-melting | 1273 | 720 | 208 | 19.4 | | 79 |
| $LaFe_{11.5}Si_{1.5}$ | arc-melting | 1323 | 300 | 205 | | | 1 |
| $LaFe_{11.5}Si_{1.5}$ | arc-melting | 1323 | 168 | 200−340 | | | 13 |
| $LaFe_{11.5}Si_{1.5}$ | arc-melting | 1423 | 168 | | 25.19 | 197.95 | 91 |
| $LaFe_{11.5}Si_{1.5}$ | arc-melting | 1373 | 960 | 194 | 23.7 | | 76 |
| $LaFe_{11.5}Si_{1.5}$ | arc-melting | 1273 | 720 | 195 | 24.6 | | 77 |
| $LaFe_{11.5}Si_{1.5}$ | | | | 194 | 24.8 | | 2 |
| $LaFe_{11.6}Si_{1.4}$ | arc-melting | 1503 | 5 | 197.6 | 18.7 | | 7 |
| $LaFe_{11.6}Si_{1.4}$ | arc-melting | 1573 | 1 | 190 | 17.5 | | 65 |
| $LaFe_{11.6}Si_{1.4}$ | arc-melting | 1523 | 5 | 190 | 25.3 | | 92 |
| $LaFe_{11.6}Si_{1.4}$ | arc- melting | 1373 | 24 | 202 | | | 93 |
| $LaFe_{11.6}Si_{1.4}$ | | 1423/1523 | 1.5/4.5 | 200 | 24.7 | | 94 |
| $LaFe_{11.6}Si_{1.4}$ | | | | 188 | 24.7 | | 2 |
| $LaFe_{11.7}Si_{1.3}$ | | | | 183 | 26.0 | | 2 |
| $LaFe_{11.8}Si_{1.2}$ | arc-melting | 1373 | 720 | 186 | 3.1 | | 56 |
| $LaFe_{11.83}Si_{1.17}$ | | | | 175 | 27.8 | | 2 |

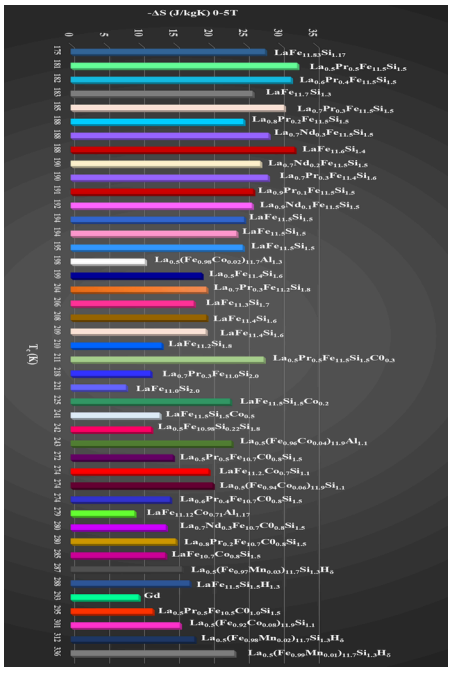


Figure 10. Curie temperature ($T_c$) vs change in entropy ($\Delta S_M$) of different $La(Fe,Si)_{13}$-based materials.[2,60,76−88]

purity of the components used for alloying as well as the atmosphere in which the experiment is carried out. Melting and annealing should take place in an argon atmosphere or a secondary vacuum. However, in order to produce a significant number of samples for magnetic refrigeration use, the annealing treatment must be done for a long time or at a high temperature, which is expensive. As a result, numerous alternative synthesis processes have been devised to shorten the annealing time. To reduce the diffusion route, they primarily rely on a reduction in particle size and close contact between the various phases formed during casting.[67]

From the literature, it is evident that most of the methods used for preparation of magnetocaloric $La(Fe,Si)_{13}$ are physical- or vacuum-based deposition methods which are not cost-effective.[3] The commercialization of magnetic refrigeration or scaling up to an industrial level needs low-cost methods to be employed.

## 7. MELT SPINNING

The production of the desired phase of $La(Fe,Si)_{13}$ can also be accomplished by a method known as melt spinning, which is an alternate and efficient procedure.[1] Most recently, melt spinning has been used in the production of $La(Fe,Si)_{13}$ ribbons as a manufacturing method. Melt spinning is an alternative and efficient approach for generating the desired phase of $La(Fe,Si)_{13}$ with minimal annealing time and heat treatment because the development of the 1:13 phase can substantially accelerate in the rapid solidification process and peritectoid relation. This makes melt spinning an alternate and efficient route for manufacturing the phase of $La(Fe,Si)_{13}$.[93] In comparison to those found in ordinary bulk alloys, the Curie transition temperature of the melt-spun-type $La(Fe,Si)_{13}$ ribbons is higher, and the magnetic and thermal hystereses are reduced.[12]

The process of melt spinning produces a refined microstructure, increased solute solubility, decreased macro and micro segregation, and the generation of metastable phases which is represented in Figure 12.[95] In melt-spun $LaFe_{13-x}Si_x$


https://doi.org/10.1021/acsomega.3c08622
ACS Omega 2024, 9, 11110−11128

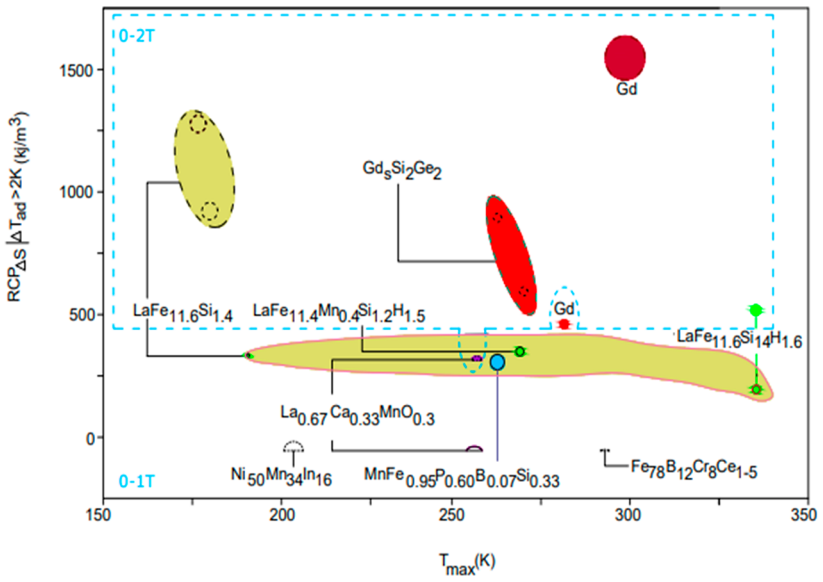


**Figure 11.** Relative cooling power of different families of magnetocaloric materials. Reprinted with permission from ref 89. Copyright 2017, IOP Publishing.

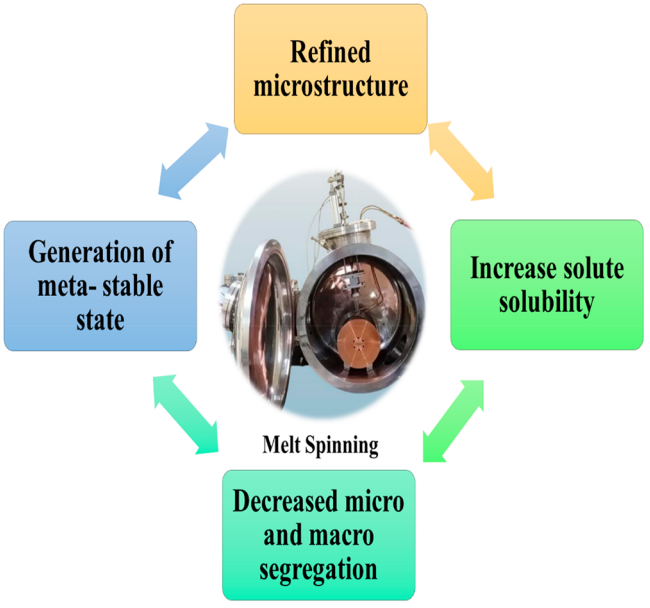


**Figure 12.** Properties of melt-spun materials.

ribbons, the reduction of synthesis time, temperature, and/or field hysteresis is practically overcome, which enables the possibility of quick magnetic cycling without a reduction in efficiency.[96]

The melt spinning method may homogenize the microstructure[93] and shorten the formation period of the 1:13 phase, in addition to being effective for grain refinement.[66] The process of developing $La(Fe,Si)_{13}$ alloys by the melt spinning technique is shown in Figure 13. According to findings by Yan et al. and Liu et al., the $NaZn_{13}$ type structure of the $LaFe_{13-x}Si_x$ compound was generated by melt spinning and subsequent annealing between 1273 and 1323 K in a short annealing time (20 min to 2 h).[6,65] Previous research indicates that reducing the amount of the nonmagnetic element Si present in the compound while maintaining its cubic $NaZn_{13}$ type structure not only improves the first-order nature of the magnetic transition but also increases magnetization, which results in a significant change in magnetic entropy. This is because decreasing the amount of the nonmagnetic element Si in the compound keeps the compounds in a cubic $NaZn_{13}$ type structure. In the aforementioned temperature range, $LaFe_{11.8}Si_{1.2}$ ribbons produced a magnetic entropy change with a value that was significantly greater than that of bulk $LaFe_{11.44}Si_{1.56}$ alloy (23 J/(kg K) at 195 K).[12] The Curie transition temperature of an alloy composed of $LaFe_{11.27}Si_{1.43}$ is 192 K in bulk but 210 K in ribbons with the same composition. This is because the rapid cooling rate during melt spinning

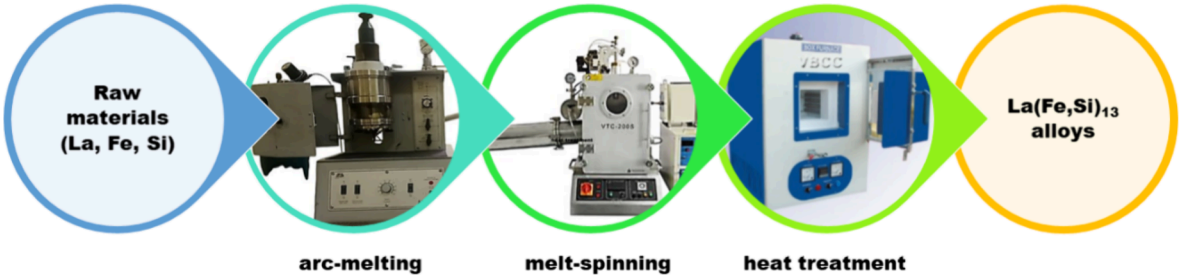


**Figure 13.** Flowchart showing the process of developing melt spun $La(Fe,Si)_{13}$ alloys. Reproduced or adapted with permission from refs 98 and 99. Copyright 2023 MTI, Vbcc.



https://doi.org/10.1021/acsomega.3c08622
ACS Omega 2024, 9, 11110−11128

Table 3. Role of Wheel Speed, Annealing Time, and Annealing Temperature on Curie Transition Temperature, Change in Entropy, and Relative Cooling Power of Different Compositions of $LaFe_{13-x}Si_x$ via Melt-Spinning Technique

| composition | wheel speed (m/s) | annealing temperature (K) | annealing time (h) | Curie temp (K) | magnetic entropy (J/(kg K() | relative cooling power (J/kg) | ref |
|---|---|---|---|---|---|---|---|
| $LaFe_{11.2}Si_{1.8}$ | 40 | 1323 | | 231 | 10.3(0−5 T), 2.7(0−1 T) | | 12 |
| $LaFe_{11.4}Si_{1.6}$ | 40 | 1323 | 2 | 222 | | | 12 |
| $LaFe_{11.5}Si_{1.5}$ | 35 | 1273 | 0.033 | 189 | 12 | | 1 |
| $LaFe_{11.5}Si_{1.5}$ | 35 | 1273 | 2 | 201 | 17 | | 1 |
| $LaFe_{11.5}Si_{1.5}$ | 35 | 1300 | 5 | 195 | 2.92 | | 100 |
| $LaFe_{11.57}Si_{1.43}$ | 40 | 1323 | 2 | 210 | 21.2 | | 97 |
| $La_{11.57}Si_{1.43}$ | 20 | 1273 | 1 | 198 | 17.8 | | 97 |
| $La_{11.57}Si_{1.43}$ | 40 | 1273[1] | 1 | 210 | 43−162(0−2 T), 83−193 (0−5 T) | | 97 |
| $LaFe_{11.6}Si_{1.4}$ | 30 | 1323 | 2 | 185 | | | 101 |
| $LaFe_{11.6}Si_{1.4}$ | | 1373 | 24 | 199 | 10.03 | | 1 |
| $LaFe_{11.6}Si_{1.4}$ | | 1323 | 0.5 | 223 | 6.30 | | 1 |
| $LaFe_{11.6}Si_{1.4}$ | | 1323 | 4 | 213 | 8.13 | | 1 |
| $LaFe_{11.6*1.1}Si_{1.4}$ | 10 | 1523 | 5 | 190.5 | 17.2 | 146.2 | 66 |
| $LaFe_{11.6*1.2}Si_{1.4}$ | 10 | 1523 | 5 | 177.4 | 13.2 | 105.6 | 66 |
| $LaFe_{11.8}Si_{1.2}$ | 40 | 1323 | 2 | 195 | 31 | | 12 |
| $LaFe_{12}Si$ | 40 | 1323 | 2 | 195 | 25.4 | | 12 |

causes more silicon to dissolve in the 1:13 phase in materials that are of the melt-spun type.[64]

The phase development and microstructure of melt-spun ribbon was investigated by Hou et al.[66] In addition, the group investigated the surface that was away from the copper wheel during the solidification process (side 1) and the surface that was in contact with the wheel (side 2), and they found that these two surfaces had different phase compositions. On side 1, there is no 1:13 phase present in the as spun state, whereas on side 2, 1:13 is the predominant phase.[1]

According to Chen et al., melt-spun $LaFe_{11.6}Si_{1.4}$ ribbons do not exhibit improved magnetocaloric capabilities because of the fine grain $\alpha$-Fe phase. On the other hand, the magnetocaloric impact becomes weak as a result of the decreased 1:13 phase fraction and higher grain boundary density.[7,66] $LaFe_{11.8}Si_{1.2}$ ribbons at 201 K under 5 T produced a very high magnetic entropy change value of 31 J/(kg K).[64] In melt spun ribbons of a certain composition created at 20 and 40 m/s wheel speed, Lyubina et al. discovered that the annealed $LaFe_{11.57}Si_{1.43}$ alloy has a Curie transition temperature, $T_c$, of 192 K. $T_c$ is enhanced to 198 and 210 K in the melt-spun ribbons.[97] An analysis of the effects of wheel speed, annealing time, and annealing temperature on the Curie transition temperature, change in entropy, and relative cooling power of $LaFe_{13-x}Si_x$ with varying compositions using the melt-spinning technique is given in Table 3.

Although the annealing process is greatly simplified by melt spinning, it is difficult to employ in large production, and ribbon samples cannot be straightened for real-time refrigeration application.[6] Normal stoichiometric melt-spun $LaFe_{13-x}Si_x$ ribbons include fewer 1:13 phases and MCE than arc-melting $LaFe_{13-x}Si_x$ buttons do. A small grain microstructure is produced by the rapid rate of solidification of the melt spinning process.[66]

Despite its technological importance, a thorough understanding of the development of the 1:13 phase in melt-spun La−Fe−Si alloy and its creation process is still missing. These characteristics have a tight connection to the solidification process and microstructure. During the process of melt spinning, the parts of the molten material that are in direct contact with the wheel solidify at a much faster pace than the remaining areas of the melt, and there is a gradient in the cooling rate across the thickness of the molten material. A ribbon that has solidified exhibits structural inhomogeneities including chemical segregation, irregular crystal nucleation distributions, and different degrees of structural relaxation. The final crystal microstructure and size are not uniform across the material, and this nonuniform structure causes some parts of the ribbon to have a lower temperature threshold for crystallization.[1]

## 8. SOME OTHER METHODS FOR ENHANCING THE MCE OF $La(Fe,Si)_{13}$

A great deal of work has gone into alloying, which may be divided into three groups: (1) rare earth elements, such as Pr, Ce, and Cd, (2) transition metals, such as Co, Ni, and Cu, and (3) light elements, such as N, H, B, and C, functioning as interstitial atoms.[102]

The characteristics of magnetocaloric $La(Fe,Si)_{13}$ alloys have been[73] improved using a number of methods, including partial element replacement, atom insertion, and provision of additional pressure through hydrogenation.[64] The substantial entropy shift in LaFeSi hydrides may be adjusted according to the hydrogen concentration, and because the itinerant-electron meta magnetic transition is weaker after hydrogenation, both thermal and magnetic hysteresis are noticeably decreased.[92] The $LaFe_{13-x}Si_x$ hydride was found to be one of the most promising candidates for the near-room-temperature magnetic refrigeration after Fujita and other researchers studied the effect of interstitial hydrogen on $LaFe_{13-x}Si_x$ alloys.[125] It was discovered that $T_c$ of the $LaFe_{13-x}Si_x$ alloys could be adjusted to near room temperature by hydrogenation while still maintaining the large magnetocaloric effect.[4]

The $LaFe_{13-x}Si_x$ alloy's $T_c$ can be raised by substituting certain elements or by inserting interstitial C or H atoms: for instance, replacing Fe with Co. However, the entropy change decreases when the phase transition shifts from a first-order magnetic transition (FOMT) to a second-order magnetic transition (SOMT). The temperature-dependent entropy curve's wider temperature range, higher relative cooling


https://doi.org/10.1021/acsomega.3c08622
ACS Omega 2024, 9, 11110−11128

power (RCP), and little thermal or magnetic hysteresis are benefits of elemental substitution.[61]

Samples of $La_{1-y}Tb_yFe_{11.5}Si_{1.5}$ were synthesized by Imam et al., who then investigated the structure, phase component, phase transition, and magnetic behavior of these materials to see how they were affected by the presence of Tb.[91] A minor strengthening of the first-order transition and an increase in the magnetic entropy change resulted from the replacement of less than 10% Tb for La. $T_c$ is not considerably impacted by Tb replacement up to 10%, but it rises when the Tb concentration is increased.[33] It is conceivable to employ Tb to modify the magnetocaloric performance of LaFeSi for magnetic refrigeration, since the compound with a small concentration of Tb replacement exhibits a promising magneto caloric performance with adequate RCP.[91]

In $La(Fe,Si)_{13}$, Chen et al. investigated how the presence of cerium (Ce), cobalt (Co), and boron (B) affected the creation of the $LaCo_{13}$ structural phase.[103,107] Based on the results of their XRD investigation, they found that the 1:13 phase in as-cast $LaFe_{11.6-x}Co_xSi_{1.4}$ alloys can only be improved by Co after it reaches a particular quantity.[104] In $LaFe_{13-x}Si_x$ alloys, the use of Ce in place of La has the potential to either speed up the alloys formation process or shorten the annealing period. In the $CeFe_{13-x}Si_x$ ($2.4 < x < 2.6$) structure with $x = 0.33$,[105] the amount of 1:13 is almost the same as in the other as-cast $La_{1-x}Ce_xFe_{1.5}Si_{1.5}$ alloys, and there is a certain amount of $Ce_2Fe_{17}$ phase when $x$ reaches 0.5, which indicates that the substitution of Ce for La in as-cast $La_{1-x}Ce_xFe_{1.5}Si_{1.5}$ alloys has some limits. In addition, the amount of 1:1:1 is not possible for the addition of Co to shorten the annealing time or improve the speed of the diffuse iron. In as-cast $LaFe_{11.6-x}B_xSi_{1.4}$ and $LaFe_{11.6}Si_{1.4}B_x$ alloys, B has the potential to enhance the production of the 1:13 phase, which is often accompanied by the $Fe_2B$ phase.[106,107]

In order to create materials with different Curie transition temperatures, Katter et al. used powder metallurgy to prepare a variety of $La(Fe,Co,Si)_{13}$-based alloys. Later, they were able to produce magnetocaloric materials with a sandwich-like shape.[49,114] The doping of transition metals in $La(Fe,Si)_{13}$ systems has been the subject of multiple investigations with the goals of enhancing MCE, lowering thermal hysteresis, and modifying the $T_c$. Antiferromagnetic coupling has been found to reduce $T_c$ when elements with atomic numbers less than that of Fe are doped at the Fe site, while increasing $T_c$ when elements with atomic numbers greater than that of Fe are doped at the Fe site.[59] There are several publications on the impact of rare earth doping, specifically Ce, Pr, and Nd, on the magnetocaloric characteristics of La−Fe−Si systems. On the other hand, adding B and C to $LaFe_{0.9}Si_{0.1}$ raises the Curie transition temperature and produces a huge MCE and a first-order magnetic transition.[32] $T_c$ increases as a result of the addition of Co, according to Yan et al. and Liu et al.[33,49] The effect of Mn addition on the MCE and Curie transition temperature of $La(Fe,Si)_{13}$ type alloys has recently been studied.[17] It has been shown that the $T_c$ and $\Delta S_M$ drop when Mn is substituted for iron.[17] There have been reports of more efficient ways that allow $T_c$ to rise. The hydrogenation causes the Curie transition temperature to rise by an order of 100 K without changing the nature of the magnetic phase transition; hence, the $\Delta S_M$ did not decline as a result.[49] Gallium (Ga) content is shown to increase with a drop in the thermal hysteresis value, indicating a weaker first-order transition. $T_c$ increases from 188 to 219 K as Ga concentration increases. In $La_{1.3}Fe_{1.6-x}Si_{1.4}Ga_x$ (x = 0.1, 1.3, 0.5), Archana et al. found that when Ga content increased from 0.1 to 0.5, the secondary phase increased and $T_c$ increased from 188 to 219 K, but $\Delta S_M$ decreased from 12.3 to 1.35 J/(g K).[59]

Chen et al. investigated the effects of varying Fe concentrations on the phase relation, microstructure, and magnetic characteristics of the compound $LaFe_{11.6}Si_{1.4}$.[66] As a result, $LaFe_{x-11.6}Si_{1.4}$ ($x$ = 0.96, 0.98, 1.0, and 1.02) prepared by arc melting and then annealing at 1423 K (1.5 h) + 1523 K (4.5 h) shows $\Delta S_M(T,H)$ values under low magnetic field (0−2 T) were found to be 15.3, 16.8, 17.9, and 24.7 J/(kg K) with an increase in Fe content from $x$ = 0.96 to 1.02, respectively.[108] As an illustration, $LaFe_{13-x}Si_x$ with the addition of C, H, or B elements, the Curie transition temperature ($T_c$) may be brought down to ambient temperature while also resulting in a little hysteresis loss. The replacement of rare earth elements, such as Pr, Nd, Ce, and Er for La, can boost the isothermal magnetic entropy change, $\Delta S_M$, and adiabatic temperature change $T_{ad}$ due to its itinerant-electron metamagnetic (IEM) transition.[33] The rare earth $\alpha$-Fe exchange coupling largely depends on the kind of rare earth, and magnetic rare earth elements have been substituted at the La site to adjust the phase transition temperature and lower the critical field of the 3d-metamagnetic transition. The field-induced magnetic transition near $T_c$ is likewise eliminated when La is replaced with another rare earth element, which changes the transition from first order to second order.[9,110]

The ball milling (BM) method is a significant component of the solid-state alloying process and is well-known for its adaptability in the production of metastable systems.[24] By employing this method of synthesis, a broad range of equilibrium and nonequilibrium alloys have been created, with the process beginning with the blending of elemental powders or particles that have already been alloyed. BM has long been utilized to create materials having a high MCE. The demagnetizing field effect and the multiphase character, which influence as-milled samples, were previously updated among the several parameters determining MCE response in BM powders. By using the BM technique, one can mix the elements with low miscibility, which is an advantage of BM techniques compared to other mixing techniques. As a consequence of this, it is possible to use it as the initial step in the process of generating a homogeneously mixed alloy that, after undergoing the appropriate annealing, will result in the formation of an intermetallic phase.[109] However, up to now, this approach has not been applicable to the synthesis of $La(Fe,Si)_{13}$ compounds beginning with raw metal powders as the starting material. The effects of ball milling on the annealing time and magnetic properties of the $LaFe_{13-x}Si_x$ compound were investigated in a study carried out by Phejar et al. The Curie transition temperature of annealed, ball-milled samples is identical to that of bulk alloys and rises proportionally with the amount of silicon present in the sample.[5,24] The magnetic entropy variation of the ball-milled $LaFe_{11.4}Si_{1.6}$ compound was found to be significantly greater than that of the bulk alloy, coming in at 16.5 J/(kg K) when subjected to a shift in magnetic field strength of 0−2 T. Hydrogen absorption in $La(Fe,Si)_{13}$[110] causes $T_c$ to rise from 190 to 330 K, whereas partial replacements of Ce and Mn cause the temperature to fall below 190 K.[45]

Phejar et al. successfully synthesized $La(Fe,Si)_{13}$ by utilizing both the arc melting process and the ball milling method.[5] Additionally, they discovered that the annealing time and


https://doi.org/10.1021/acsomega.3c08622
ACS Omega 2024, 9, 11110−11128

temperature might be decreased when using the ball milling process as opposed to the arc melting approach. Ball milling only takes 30 min at 1473 K for the formation of a 1:13 phase but the arc melting method takes 30 days of annealing at 1473 K. Additionally, magnetic experiments reveal that in a field of 0−5 T, the $\Delta S_M$ values for $x$ = 1.4 and 1.6 are 32.6 and 25 J/(kg K), respectively. These values surpass the comparable bulk compounds' values of 24 and 18 J/(kg K), respectively.[111] For variations in magnetic field strength ranging from 0−2 to 0−5 T, the RCP values of $LaFe_{11.4}Si_{1.6}$ are 155 and 439 J/kg, respectively. However, the brittle nature of $La(Fe,Si)_{13}$-based alloys makes it extremely difficult to produce a significant surface area. Some of the benefits of using melt spinning, pulverization, and hot pressing (HP) to create $La(Fe,Si)_{13}$-based materials include the reduction of internal stress and the prevention of crushing caused by the magneto volume effect. To this end, a variety of binders have been used, including Pd-based amorphous alloys, Cu, Sn, $Sn_{42}Bi_{58}$, Bi, In, and epoxy resin.[5,24]

For better magnetic performance, NdFeB magnets are often treated using the HP method.[66] Likewise, to get compounds based on $La(Fe,Si)_{13}$ with desirable MCE characteristics, Zhong et al. combined heat pressing and grain boundary diffusion (GBD). The Curie transition temperature ($T_c$) of the $La(Fe_{11.6},Si_{1.4})$/La−Co magnetocaloric composite ranges from 1973 to 235 K as a result of the diffusion of Co in the $NaZn_{13}$-type (1:13) predominant phase.[61] As the diffusion time is increased, the maximum magnetic entropy change ($\Delta S_M$) at 2 T initially rises from 5.62 to 7.60 J/(kg K).[61,112]

Researchers have studied the corrosion of the $La(Fe_{0.94}Co_{0.06})_{11.7}Si_{1.3}$ compound and $LaFe_{11.6}Si_{1.4}$ alloy in a variety of fluids.[92] The findings demonstrate that the use of these alkaline solutions is required to guarantee the formation of a protective film on the metal's surface and to have a decent inhibitory effect on the $LaFe_{13-x}Si_x$ compounds under certain conditions. It was hypothesized by Ipus et al. that the $La(Fe,Si)_{13}$ phase concentration might be increased without melting the sample.[56] The findings demonstrate that grinding and particle size selection can boost the proportion of the fcc-$La(Fe,Si)_{13}$ and, in turn, the magnetocaloric effect reaction relative to the original bulk sample.[23,56] So far as we are aware, $La(Fe,Si)_{13}$ alloys cannot be cast in large quantities. Melt spinning has been used to refine the primary Fe phase, while powder metallurgy (HDSH)[69] has been used to insert hydrogen atoms into alloys, although these processes produce a powder and/or ribbon rather than a solid material.

By using thermally induced breakdown and recombination of the 1:13 phase,[16] it is possible to solve the issues that arise during the machining of bulk materials. In their study, the influence of the thermal decomposition reaction on the mechanical and magnetocaloric properties of $La(Fe,Si,Co)_{13}$ was examined by Lowe et al.[113,114] They determined that temperatures between 973 and 1073 K are optimal for inducing the thermal decomposition reaction in $La(Fe,Si,Co)_{13}$ sintered samples.[114] This conclusion was reached on the basis of the observation that the thermal decomposition reaction had an impact on the compound's mechanical properties.[113] On the other hand, this results in a reduction in the magnetocaloric effect that the material possesses,[39] but at the same time it raises the material's mechanical property and, as a result, makes it easier to machine.[21,114]

## 9. THEORETICAL STUDIES ON $La(Fe,Si)_{13}$

For the successful development of magnetic cooling technology, basic research on the fundamental properties, electronic structure, and understanding of magnetism is just as important as experimental studies of magnetic and magnetocaloric properties. In order to modelize the experimental isotherms of magnetization as a function of both magnetic field and temperature $M(H,T)$, the basic formulation of the theoretical approach uses a scaling strategy based on the mean-field theory combined with the Bean−Rodbell model and Landau theory. The following section gives a glimpse of the theoretical modeling of $LaFe_{13-x}Si_x$.[115]

**9.1. Landau Theory of Phase Transitions.** The significant magnetocaloric effect of FOMT systems is explained by Landau theory, which additionally describes the influence of magnetic irreversibility on the estimation of the magnetocaloric effect from magnetization measurements and the magnetoelastic coupling effect on MCE on ferromagnetic materials.

This model begins with the Gibbs free energy ($G$) expansion

$$G(T, M) = G_0 + \frac{1}{2}A(T)M^2 + \frac{1}{4}B(T)M^4 + \frac{1}{6}C(T)M^6 - MH \tag{3}$$

where $A$, $B$, and $C$ represent the Landau coefficients that depend on temperature.

The Curie transition temperature $T_c$ of the system is often determined by assuming that $A$ has a linear temperature:

$$A(T) = A'(T - T_c) \tag{4}$$

In the susceptibility regime, this linear relationship is valid and complies with the Curie law

$$\frac{H}{M} = \frac{C_{Curie}}{T - T_c} \tag{5}$$

where $C_{Curie}$ denotes the system's Curie constant.

The inverse Curie constant is then equal to the $A'$ parameter for low $M$ values. Then eq 3 becomes

$$\frac{H}{M} = A(T) + B(T)M^2 + C(T)M^4 \tag{6}$$

This resulting equation allows us to visualize $\frac{H}{M}$ versus $M^2$, often known as the Arrot plot, and use magnetization data to calculate the Landau coefficient's temperature dependence.

The magnetization does not saturate even at extremely low temperatures when the system reaches greater values of $M$, which is one of the main drawbacks of Landau's theory. Furthermore, the values of Landau's parameters $B$ and $C$ do not provide any profound physical understanding. In order to overcome the existing drawbacks, the Bean-Rodbell model can be employed.[116]

**9.2. Bean−Rodbell Model.** The Bean−Rodbell model was initially established in a study on the magnetic characteristics of MnAs alloy which exhibits a large magneto-volume coupling effect. Several of the Landau theory's drawbacks are addressed by this model.

A linear relationship between Curie transition temperature ($T_c$) and volume is imposed by this model as

$$T_c = T_0\left(1 + \beta\left(\frac{V - V_0}{V_0}\right)\right) \tag{7}$$



https://doi.org/10.1021/acsomega.3c08622
ACS Omega 2024, 9, 11110−11128

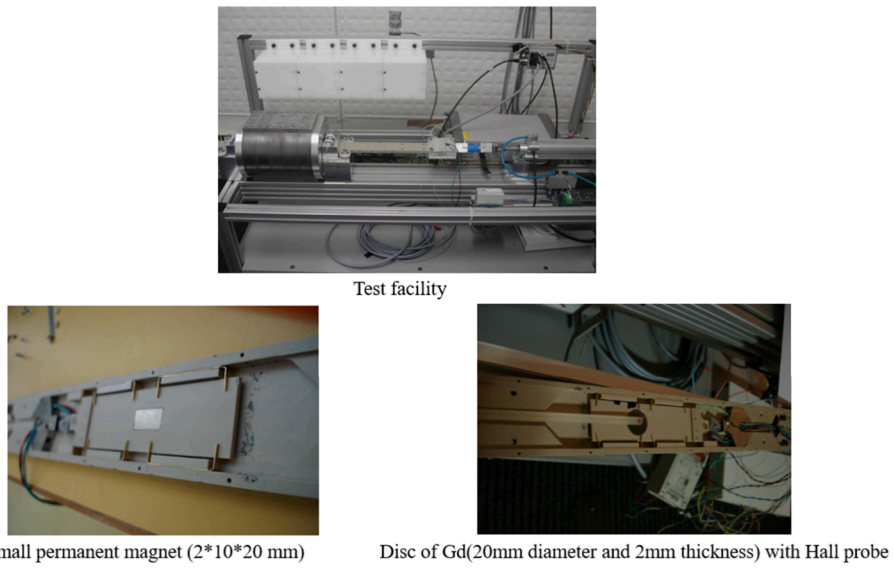


**Figure 14.** Test facility with a magnetic field source of 2T by Sari et al.[119] Photograph courtesy O. Sari. Copyright 2009.

where $V$ represents the volume, $\beta$ is positive and constant, and $V_0$ is the equilibrium volume in the absence of magnetic interactions.

The magnetic transition becomes first-order with a strong enough linear dependence of $T_c$ on volume and large $\beta$ value. The $\eta$ parameter establishes the crossover point as

$$\eta = 40Nk_BKT_0\beta^2\frac{(S(S+1))^2}{(2S+1)^4-1} \quad (8)$$

Here, $N$ stands for spin density, $S$ for spin quantum number, $k_B$ for Boltzmann constant and $K$ for compressibility. When $\eta < 1$ the magnetic transition is second order and when $\eta > 1$ the magnetic transition is first order.

It is also important to note that, in contrast to the Landau theory of phase transitions, a quantitative analysis of experimental data using the Bean−Rodbell model is feasible for both FOMT and SOMT systems. This is because physically significant parameters like spin and compressibility are defined in the model. Using this model, simulations may be performed at low computing cost, and disordered SOMT and FOMT systems can be described by taking into account smooth distributions of $T_c$ values with hundreds of points.[117]

## 10. SOME PROTOTYPES WITH La(Fe,Si)$_{13}$-BASED MATERIALS

Materials based on La(Fe,Si)$_{13}$ are being eyed as a possible solution for room-temperature magnetic refrigeration because their synthesis is benign to the environment, does not necessitate high-purity or expensive raw materials, and increases the efficiency and temperature span of refrigeration devices.[2] The following paragraphs detail the advancement in room-temperature magnetic refrigerator prototype through the years.

At the Baotou Research Institute of Rare Earth in China, a reciprocating room-temperature magnetic refrigerator prototype was unveiled in 2006. A permanent magnet, a cold accumulator, an AMR bed, a driving pump, and a heat exchanger made up the prototype. The machine contained 200 g of $LaFe_{10.97}Co_{0.78}Si_{1.05}B_{0.2}$ and 750 g of gadolinium as magnetic refrigerants, and the magnetocaloric material particles ranged in size from 0.5 to 2 mm. As a heat transfer fluid, an alkalescent water solution with a pH of 10 was used. The magnetic structure provided a maximum magnetic field intensity of 1.5 T and had an air gap with a diameter of 34 mm and a length of 200 mm. At a frequency of 0.18 Hz, the system achieved a maximum no load temperature spread of 18 °C. 20 W of cooling power was available with a 5 °C temperature range. After 45 min of operation, this state was attained.[118]

In 2009, Western Switzerland University of Applied Sciences created reciprocating equipment to characterize magnetocaloric materials (Figure 14). Fe−Nd−B permanent magnets generated a 2 T air gap magnetic field. A holder moved the magnetocaloric material in and out of the magnetic field. Pulsed air transferred heat. $LaFe_{11}Co_{0.9}Si_{1.1}$ and Gd were utilized to test the equipment, detecting the magnetocaloric material temperature change under adiabatic and nonadiabatic conditions. The device could determine the temperature change of the tested materials for varied applied magnetic fields.[119]

Batou Research Institute of Rare Earth demonstrated their second reciprocating magnetic refrigeration testing unit in 2013. The identical 1.5 T Nd−Fe−B permanent-magnet assembly moved over two AMR beds. The operating frequency increased to 0.9 Hz. They investigated three AMRs with three magnetocaloric materials: Gd, $LaFe_{11.0}Co_{0.9}Si_{1.1}B_{0.25}$ ($T_c$ = 291 K), and $LaFe_{11.08}Co_{0.82}Si_{1.1}B_{0.25}$ ($T_c$ = 279 K). AMRs have packed beds with particle sizes between 0.42 and 0.85 mm. Both AMRs used a single material, one with Gd and the other with La−Fe−Co−Si−B ($T_c$ = 291 K). The third was a two-layer La−Fe−Co−Si−B AMR. Both La−Fe−Co−Si−B-based AMRs weighed 580 g. The Gd AMR weighed 785 g.[120]

To study the cooling load under various $\Delta T$ spans, Tusek et al. tested their AMR in 2013 using a system that was outfitted with a reciprocating magnet and a heat exchanger.[121] They have noted that the maximum $\Delta T$ span changes with the operating frequency $P$ and the utilization factor $U$. When compared to Gd, it is bigger for LaFeSi-based AMR at low $U$ values ($\Delta T$ span), while Gd's grows with higher $U$ values. The hot side temperature also affects the maximum $\Delta T$ span, which


https://doi.org/10.1021/acsomega.3c08622
ACS Omega 2024, 9, 11110−11128

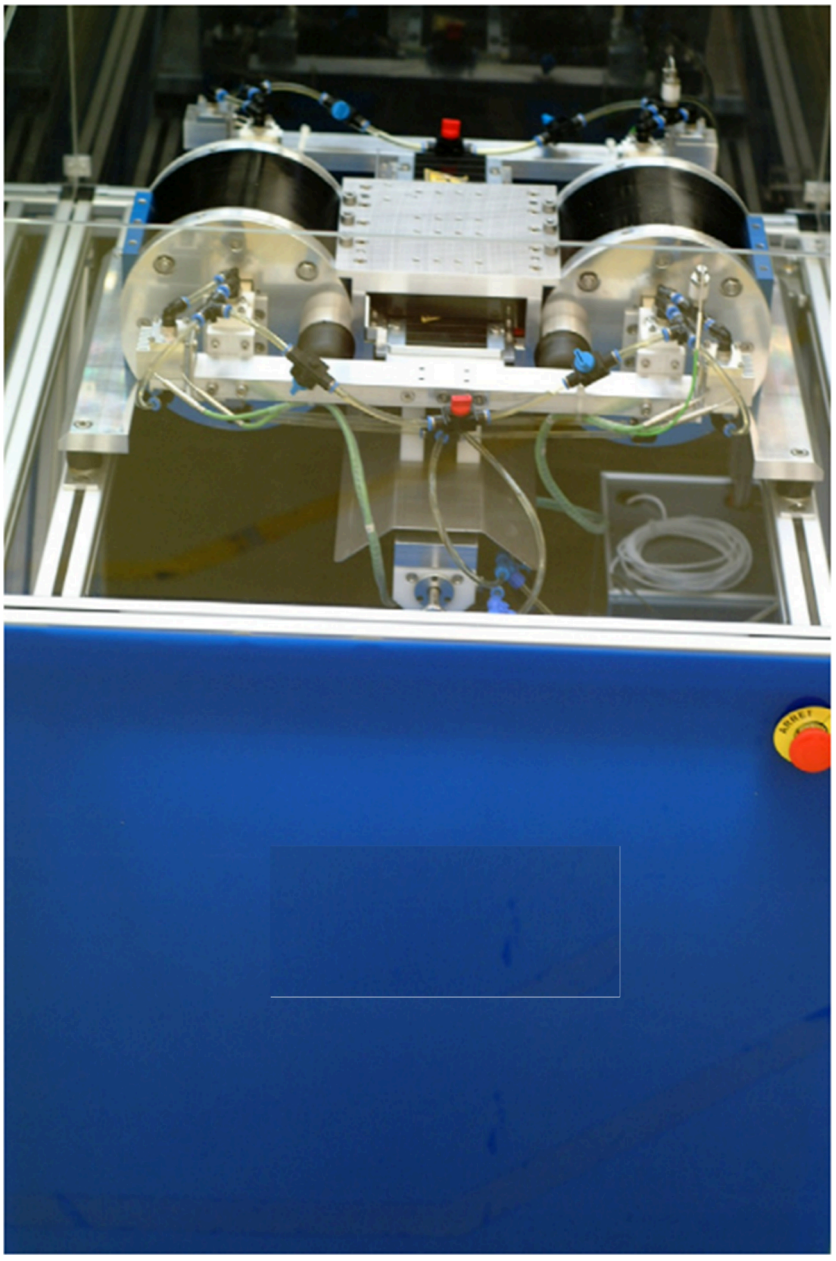

**Figure 15.** Developed prototype of magnetic cooling machine by Balli et al. in 2012. Reprinted with permission from ref 122. Copyright 2012, Elsevier.

is greatest at 35 °C for Gd, 27 °C for a two-layered structure, and 43 °C for a seven-layered $La(Fe,Co,Si)_{13}$ structure.[121]

Balli et al. created a prototype in 2012 with two AMRs that alternately magnetize and demagnetize to lessen magnetic forces on the magnetic refrigerant (Figure 15). The applied magnetic field limits the demagnetization field. They found that two AMRs, one with Gd and the other with a $La(Fe,Co,Si)_{13}$ composite, had comparable maximal $\Delta T$ spans of 14 and 16 K. They examined La−Fe−Co−Si compounds in aqueous solutions with a corrosion inhibitor and silicon oil. 3% noxal antioxidant gave the best corrosion resistance. Water is better for fluid heat transmission than Si oil ($C_p$ = 1.6 J/(g K)).[122]

## 11. CONCLUDING REMARKS

In this work, a detailed analysis of current trends and future materials for magnetic refrigeration application is presented, with the primary focus being placed on $LaFe_{13-x}Si_x$-based compounds. After reviewing a concise history of the evolutionary process of these materials, one can deduce that the area is still in its infancy and calls for labor that is meticulous and methodical.[123,124] The various approaches to synthesis were discussed, and comparisons were drawn between them. The development of MCE has been detailed, with a particular emphasis placed on $La(Fe,Si)_{13}$ for applications involving magnetic refrigeration.[125] During the course of the synthesis, we brought attention to a number of issues that may potentially arise, such as oxidation, tweaking the Curie transition temperature to be close to ambient temperature, etc. Methods that involve the chemical substitution of La, Fe,



https://doi.org/10.1021/acsomega.3c08622
ACS Omega 2024, 9, 11110−11128

and Si with other elements, as well as the insertion of light elements like hydrogen, are preferable approaches for overcoming these challenges. The progress that has been made in this regard is quite encouraging, and it is anticipated that $La(Fe,Si)_{13}$ composites manufactured using these techniques may in the near future provide a viable alternative to traditional refrigeration.

## AUTHOR INFORMATION


### Corresponding Author

**Madhuri Wuppulluri** − *Ceramic Composites Laboratory, Centre for Functional Materials, Vellore Institute of Technology, Vellore 632014 Tamil Nadu, India;* orcid.org/0000-0002-1650-9931; Phone: +91-8754548779; Email: madhuriw12@hotmail.com

### Authors

**Anjana Vinod** − *School of Advanced Sciences, Vellore Institute of Technology, Vellore 632014 Tamil Nadu, India*

**D. Arvindha Babu** − *Defence Metallurgical Research Laboratory, Hyderabad 500058 Telangana, India*

Complete contact information is available at: https://pubs.acs.org/10.1021/acsomega.3c08622


### Notes

The authors declare no competing financial interest.

## ACKNOWLEDGMENTS

The authors acknowledge SAS, VIT University, for providing financial support and research facilities for the work.

## REFERENCES


(1) Hou, X.; Lampen-Kelley, P.; Xue, Y.; Liu, C.; Xu, H.; Han, N.; Ma, C.; Srikanth, H.; Phan, M. H. Formation Mechanisms of NaZn13-Type Phase in Giant Magnetocaloric La-Fe-Si Compounds during Rapid Solidification and Annealing. *J. Alloys Compd.* **2015**, *646*, 503−511.

(2) Shen, B. G.; Sun, J. R.; Hu, F. X.; Zhang, H. W.; Cheng, Z. H. Recent Progress in Exploring Magnetocaloric Materials. *Adv. Mater.* **2009**, *21* (45), 4545−4564.

(3) Franco, V.; Blázquez, J. S.; Ipus, J. J.; Law, J. Y.; Moreno-Ramírez, L. M.; Conde, A. Magnetocaloric Effect: From Materials Research to Refrigeration Devices. *Prog. Mater. Sci.* **2018**, *93*, 112−232.

(4) Wang, J.; Chen, Y.; Tang, Y.; Xiao, S.; Liu, T.; Zhang, E. The Hydrogenation Behavior of LaFe11.44Si1.56 Magnetic Refrigerating Alloy. *J. Alloys Compd.* **2009**, *485* (1−2), 313−315.

(5) Phejar, M.; Paul-Boncour, V.; Bessais, L. Structural and Magnetic Properties of Magnetocaloric LaFe 13-XSix Compounds Synthesized by High Energy Ball-Milling. *Intermetallics* **2010**, *18* (12), 2301−2307.

(6) Zhang, M.; Liu, J.; He, C.; Yan, A. Novel Microstructure and Large Magnetocaloric Effect in La2Fe11Si2Magnetic Refrigerant. *Mater. Lett.* **2014**, *134*, 87−90.

(7) Chen, X.; Chen, Y.; Tang, Y. The Influence of Different Cooling Processes on Phase, Microstructure, and Magnetocaloric Properties of LaFe11.6Si1.4 Compounds. *Solid State Commun.* **2014**, *186*, 56−63.

(8) Bessais, L.; Phejar, M.; Paul-Boncour, V. Structural and Magnetocaloric Properties of Ball Milled LaFe13−xSix(H,C)Y. *MRS Adv.* **2017**, *2*, 3447.

(9) Kovac, J.; Svec, P.; Skorvanek, I. MAGNETOCALORIC EFFECT IN AMORPHOUS AND NANOCRYSTALLINE FeCrNbBCu ALLOYS. *Rev. Adv. Mater. Sci.* **2008**, *18* (6), 533−535.

(10) Fan, W. B.; Hou, Y. H.; Ge, X. J.; Huang, Y. L.; Luo, J. M.; Zhong, Z. C. Microstructure and Improved Magnetocaloric Properties: LaFeSi/LaAl Magnets Prepared by Spark Plasma Sintering Technique. *J. Phys. D. Appl. Phys.* **2018**, *51* (11), 115003.

(11) Blazquez, J. S.; Ipus, J. J.; Moreno-Ramirez, L. M.; Alvarez-Gomez, J. M.; Sanchez-Jimenez, D.; Lozano-Perez, S.; Franco, V.; Conde, A. Ball Milling as a Way to Produce Magnetic and Magnetocaloric Materials: A Review. *J. Mater. Sci.* **2017**, *52* (20), 11834−11850.

(12) Gutfleisch, O.; Yan, A.; Muller, K.-H. Large Magnetocaloric Effect in Melt-Spun LaFe13−xSix. *J. Appl. Phys.* **2005**, *97*, 10M305.

(13) Feng, J.; Geutjens, R.; Thang, N. V.; Li, J.; Guo, X.; Kéri, A.; Basak, S.; Galbács, G.; Biskos, G.; Nirschl, H.; Zandbergen, H. W.; Brück, E.; Schmidt-Ott, A. Magnetic Phase Transition in Spark-Produced Ternary LaFeSi Nanoalloys. *ACS Appl. Mater. Interfaces* **2018**, *10* (7), 6073−6078.

(14) Webster, P. J. Heusler Alloys. *Contemp. Phys.* **1969**, *10* (6), 559−577.

(15) Court, C. J.; Jain, A.; Cole, J. M. Inverse Design of Materials That Exhibit the Magnetocaloric Effect by Text-Mining of the Scientific Literature and Generative Deep Learning. *Chem. Mater.* **2021**, *33* (18), 7217−7231.

(16) Ghosh, S. Study of Magnetocaloric Effect in Off-Stoichiometric Ni-Mn-Sb Heusler Compounds by Density Functional Theory and Monte Carlo Methods. Ph.D. Thesis, Indian Institute of Technology Guwahati, 2020.

(17) Tavares, S.; Yang, K.; Meyers, M. A. Heusler Alloys: Past, Properties, New Alloys, and Prospects. *Prog. Mater. Sci.* **2023**, *132*, No. 101017.

(18) Djamel-Eddine, M.; BENCHERIF, K.; BENSAID, D. First Principle Investigation of Physical Properties of MNiBi: (M = Sc, Y) Half-Heusler Compounds. *Rev. Mex. Fis.* **2022**, *68* (6), 1−11.

(19) Kanza, E. Ab-Inito Study of the Electronic and Magnetic Properties of CoXMnSi(X = Ru,Rh) Compounds. Thesis, Université de Médéa, 2018.

(20) Bahlouli, S.; Aarizou, Z.; Elchikh, M. Structure and Magnetic Properties in Ruthenium-Based Full-Heusler Alloys: Ab Initio Calculations. *Mod. Phys. Lett. B* **2013**, *27* (30), 1350219.

(21) Balke, B.; Wurmehl, S.; Fecher, G. H.; Felser, C.; Kübler, J. Rational Design of New Materials for Spintronics: Co2FeZ (Z = Al, Ga, Si, Ge). *Sci. Technol. Adv. Mater.* **2008**, *9* (1), 014102.

(22) Brück, E. Developments in Magnetocaloric Refrigeration. *J. Phys. D. Appl. Phys.* **2005**, *38* (23), R381.

(23) Shaughnessy, M.; Damewood, L.; Fong, C. Y.; Yang, L. H.; Felser, C. Structural Variants and the Modified Slater-Pauling Curve for Transition-Metal-Based Half-Heusler Alloys. *J. Appl. Phys.* **2013**, *113* (4), 043709.

(24) Phejar, M.; Paul-Boncour, V.; Bessais, L. Magnetocaloric Study of Mechanically Alloyed LaFeSi. *TMS Annu. Meet.* **2011**, *1*, 319−324.

(25) Chernenko, V. A.; L'vov, V. A.; Cesari, E.; Barandiaran, J. M. *Fundamentals of Magnetocaloric Effect in Magnetic Shape Memory Alloys*, 1st ed.; Elsevier: 2019; Vol. *28*. DOI: 10.1016/bs.hmm.2019.03.001.

(26) Fong, C. Y.; Pask, J. E. *Half-metallic Materials and Their Properties*. Imperial College Press, 2013.

(27) Gutfleisch, O.; Willard, M. A.; Brück, E.; Chen, C. H.; Sankar, S. G.; Liu, J. P. Magnetic Materials and Devices for the 21st Century: Stronger, Lighter, and More Energy Efficient. *Adv. Mater.* **2011**, *23* (7), 821−842.

(28) Smith, A.; Bahl, C. R. H.; Bjork, R.; Engelbrecht, K.; Nielsen, K. K.; Pryds, N. Materials Challenges for High Performance Magnetocaloric Refrigeration Devices. *Adv. Energy Mater.* **2012**, *2* (11), 1288−1318.

(29) Rejeb, M. B.; Cheikhrouhou-Koubaa, W.; Koubaa, M.; Cheikhrouhou, A.; Nowak, S.; Sicard, L.; Ammar-Merah, S. Annealing Effect on the Structural, Magnetic and Magnetocaloric Properties of La0.65Ca0.2K0.15MnO3 Synthesized by SolGel Method. *J. Supercond. Nov. Magn.* **2015**, *28* (4), 1379−1387.

(30) Yue, M.; Xu, H.; Zhao, J. L.; Xu, M. F.; Liu, D. M.; Zhang, J. X. Structural, Thermal, and Magnetic Properties of MnFePSiGe

Compounds Prepared by Spark Plasma Sintering Method. *J. Magn. Magn. Mater.* **2013**, *335*, 114−117.
(31) Keefe, P. Second Law Violation By Magneto-Caloric Effect Adiabatic Phase Transition of Type I Superconductive Particles. *Entropy* **2004**, *6*, 116.
(32) Zhang, M.; Ouyang, Y.; Zhang, Y.; Liu, J. LaFe11Co0.8Si1.2/Al Magnetocaloric Composites Prepared by Hot Pressing. *J. Alloys Compd.* **2020**, *823*, No. 153846.
(33) Yan, Y.; Liu, C.; Lu, W.; Sun, Y.; Zhu, W.; Nie, X.; Sang, X.; Zhao, W.; Zhang, Q. Effect of Gd Doping on the Microstructure and Magnetocaloric Properties of LaFe11.5Si1.5 Alloy. *J. Alloys Compd.* **2022**, *910*, No. 164858.
(34) *Emil_Warburg*. https://en.wikipedia.org/wiki/Emil_Warburg (accessed 2023-09-19).
(35) *Auguste_Piccard*. https://en.wikipedia.org/wiki/Auguste_Piccard (accessed 2023-07-05).
(36) *Pierre_Weiss*. https://en.wikipedia.org/wiki/Pierre_Weiss (accessed 2023-08-07).
(37) *William_Giauque*. https://en.wikipedia.org/wiki/William_Giauque (accessed 2023-08-16).
(38) *debye*. https://www.nobelprize.org/prizes/chemistry/1936/debye/facts/ (accessed 2023-10-10).
(39) Zhang, Y. Review of the Structural, Magnetic and Magnetocaloric Properties in Ternary Rare Earth RE2T2X Type Intermetallic Compounds. *J. Alloys Compd.* **2019**, *787*, 1173−1186.
(40) Keefe, P. D. Second Law Violation by Magneto-Caloric Effect Adiabatic Phase Transition of Type I Superconductor Particles. *Entropy* **2004**, *6* (1), 116−127.
(41) Jayaraman, T. V.; Boone, L.; Shield, J. E. Journal of Magnetism and Magnetic Materials Magnetocaloric Effect and Refrigerant Capacity in Melt-Spun Gd − Mn Alloys. *J. Magn. Magn. Mater.* **2013**, *345*, 153−158.
(42) Fu, S.; Long, Y.; Li, X.; Wang, C.; Chang, Y.; Ye, R.; Zhang, H. Structure and Magnetic Properties of LaFe 11.5-XCo XSi 1.5C 0.2 Compounds for Magnetic Refrigeration near Room Temperature. *J. Magn. Magn. Mater.* **2012**, *324* (22), 3842−3845.
(43) Liu, J.; Moore, J. D.; Skokov, K. P.; Krautz, M.; Löwe, K.; Barcza, A.; Katter, M.; Gutfleisch, O. Exploring La(Fe,Si)13-Based Magnetic Refrigerants towards Application. *Scr. Mater.* **2012**, *67* (6), 584−589.
(44) Bayer, N. B.; Livermore, L. The Magnetocaloric Effect & Performance of Magnetocaloric Materials in a 1D Active Magnetic Regenerator Simulation. Thesis, Wright State University, **2019**.
(45) Fujieda, S.; Fukamichi, K.; Suzuki, S. Microstructure and Isothermal Magnetic Entropy Change of La(Fe 0.89Si0.11)13 in a Single-Phase Formation Process by Annealing. *J. Alloys Compd.* **2013**, *566*, 196−200.
(46) Piazzi, M.; Bennati, C.; Curcio, C.; Kuepferling, M.; Basso, V. Journal of Magnetism and Magnetic Materials Modeling Speci Fi c Heat and Entropy Change in La (Fe − Mn − Si) 13 − H Compounds. *J. Magn. Magn. Mater.* **2016**, *400*, 349−355.
(47) Li, Z. B.; Sanchez Llamazares, J. L.; Sanchez-Valdes, C. F.; Zhang, Y. D.; Esling, C.; Zhao, X.; Zuo, L. Microstructure and Magnetocaloric Effect of Melt-Spun Ni52Mn26Ga22 Ribbon. *Appl. Phys. Lett.* **2012**, *100*, No. 174102.
(48) Barman, A.; Kar-Narayan, S.; Mukherjee, D. Caloric Effects in Perovskite Oxides. *Adv. Mater. Interfaces* **2019**, *6* (15), 1−31.
(49) Gębara, P.; Pawlik, P. Broadening of Temperature Working Range in Magnetocaloric La(Fe,Co,Si)13- Based Multicomposite. *J. Magn. Magn. Mater.* **2017**, *442*, 145−151.
(50) Hamad, M. K. A. Developing Near Room Temperature Magnetocaloric Materials. Thesis, King Fahd University of Petroleum & Minerals, 2018.
(51) Li, B.; Hu, W. J.; Liu, X. G.; Yang, F.; Ren, W. J.; Zhao, X. G.; Zhang, Z. D. Large Reversible Magnetocaloric Effect in TbCoC2 in Low Magnetic Field. *Appl. Phys. Lett.* **2008**, *92* (24), 242508.
(52) Law, J. Y.; Franco, V.; Moreno-Ramírez, L. M.; Conde, A.; Karpenkov, D. Y.; Radulov, I.; Skokov, K. P.; Gutfleisch, O. A Quantitative Criterion for Determining the Order of Magnetic Phase Transitions Using the Magnetocaloric Effect. *Nat. Commun.* **2018**, *9* (1), 2680.
(53) Gutfleisch, O.; Gottschall, T.; Fries, M.; Benke, D.; Radulov, I.; Skokov, K. P.; Wende, H.; Gruner, M.; Acet, M.; Entel, P.; Farle, M. Mastering Hysteresis in Magnetocaloric Materials. *Philos. Trans. R. Soc. A Math. Phys. Eng. Sci.* **2016**, *374* (2074), 20150308.
(54) Saidi, M.; Walha, S.; Hlil, E. K.; Bessais, L.; Jemmali, M. Effect of Chromium Substitution on Structural, Magnetic and Magnetocaloric Properties of GdFe12−xCrx Intermetallic Compounds, Mössbauer Spectrometry and Ab Initio Calculations. *J. Solid State Chem.* **2021**, *297*, No. 122019.
(55) Teran, E. M. Near Room Temperature Magnetocaloric Materials for Magnetic Refrigeration. Thesis, University of Texas at El Paso, 2019.
(56) Ipus, J. J.; Borrego, J. M.; Moreno-Ramírez, L. M.; Blázquez, J. S.; Franco, V.; Conde, A. Grinding and Particle Size Selection as a Procedure to Enhance the Magnetocaloric Response of La(Fe,Si)13 Bulk Samples. *Intermetallics* **2017**, *84*, 30−34.
(57) Talakesh, S.; Nourbakhsh, Z. Structural, Electronic, Magnetic and Thermodynamic Properties of LaFeSi, GdFeSi and TbFeSi Nano-Layers Using First-Principles Calculations. *Indian J. Phys.* **2019**, *93* (5), 571−582.
(58) Jayaraman, T. V.; Boone, L.; Shield, J. E. Magnetocaloric Effect and Refrigerant Capacity in Melt-Spun Gd-Mn Alloys. *J. Magn. Magn. Mater.* **2013**, *345*, 153−158.
(59) Ga, S. Magnetocaloric Effect, Magnetic Interactions and Phase Transition. *J. Supercond. Nov. Magn.* **2022**, No. 0123456789.
(60) Tegus, O.; Brück, E.; Buschow, K. H. J.; De Boer, F. R. Transition-Metal-Based Magnetic Refrigerants for Room-Temperature Applications. *Nature* **2002**, *415* (6868), 150−152.
(61) Zhong, X. C.; Peng, D. R.; Dong, X. T.; Huang, J. H.; Zhang, H.; Jiao, D. L.; Zhang, H.; Liu, Z. W.; Ramanujan, R. V. Improvement in the Magnetocaloric Properties of Sintered La(Fe,Si)13 Based Composites Processed by La-Co Grain Boundary Diffusion. *J. Alloys Compd.* **2019**, *780*, 873−880.
(62) Fu, S.; Long, Y.; Wang, C.; Zhang, M.; Ohnuki, S.; Hu, F.-X. Formation of 1:13 Phase in La(Fe,Si) -Based Compounds by Diffusion of LaFe,Si/a-Fe(Si)Couple. *IEEE Trans. Magn.* **2012**, *48* (11), 3757−3759.
(63) Chen, X.; Chen, Y.; Tang, Y. The Studies of High-Temperature and Short-Time Annealing, Phase Transition Process, and Magnetic Property for LaFe 11.7Si 1.3 Compound. *Phase Transitions* **2012**, *85* (1−2), 27−40.
(64) Yang, L.; Zhou, Z.; Qian, J.; Ge, X.; Li, J.; Hu, Q.; Li, J. Peritectic Solidification Path of the La(Fe,Si)13 Phase in Dual-Phase Directionally Solidified La-Fe-Si Magnetocaloric Alloys. *Metall. Mater. Trans. A Phys. Metall. Mater. Sci.* **2017**, *48* (9), 4229−4236.
(65) Liu, T.; Chen, Y.; Tang, Y.; Xiao, S.; Zhang, E.; Wang, J. Structure and Magnetic Properties of Shortly High Temperature Annealing LaFe11.6Si1.4 Compound. *J. Alloys Compd.* **2009**, *475* (1−2), 672−675.
(66) CHEN, X.; CHEN, Y.-g.; TANG, Y.-b.; XIAO, D.-q. quan. Effects of Solidification Rate and Excessive Fe on Phase Formation and Magnetoclaoric Properties of LaFe11.6xSi1.4. *Trans. Nonferrous Met. Soc. China (English Ed.* **2017**, *27* (9), 2015−2021.
(67) Paul-Boncour, V.; Bessais, L. Tuning the Magnetocaloric Properties of the La(Fe,Si)13 Compounds by Chemical Substitution and Light Element Insertion. *Magnetochemistry* **2021**, *7* (1), 13.
(68) Chen, G. Vibration Modelling and Verifications for Whole Aero-Engine. *J. Sound Vib.* **2015**, *349*, 163−176.
(69) Atanasov, R.; Ailenei, D.; Bortnic, R.; Hirian, R.; Souca, G.; Szatmari, A.; Barbu-Tudoran, L.; Deac, I. G. Magnetic Properties and Magnetocaloric Effect of Polycrystalline and Nano-Manganites $Pr_{0.65}Sr_{(0.35-x)}Ca_xMnO_3$ ($x \leq 0.3$). *Nanomaterials* **2023**, *13*, 1373.
(70) Benelli, C. *Introduction To Molecular Magnetism From Transition Metals to Lanthanides*; Wiley: 2015.
(71) Schobinger, D.; Gutfleisch, O.; Hinz, D.; Müller, K. H.; Schultz, L.; Martinek, G. High Temperature Magnetic Properties of 2:17 Sm-Co Magnets. *J. Magn. Magn. Mater.* **2002**, *242−245*, 1347−1349.


https://doi.org/10.1021/acsomega.3c08622
*ACS Omega* 2024, 9, 11110−11128

(72) Wonchala, J.; Hazledine, M.; Goni Boulama, K. Solution Procedure and Performance Evaluation for a Water-LiBr Absorption Refrigeration Machine. *Energy* **2014**, *65*, 272−284.
(73) Hu, J.; Dong, Z.; Shen, Y.; Fu, B.; Zhang, B. Effect of Excess Lanthanum on Corrosion and Magnetocaloric Property of LaFe11.5-Si1.5 Compounds. *J. Rare Earths* **2019**, *37* (10), 1116−1120.
(74) Xu, Z.; Dai, Y.; Fang, Y.; Luo, Z.; Han, K.; Song, C.; Zhai, Q.; Zheng, H. High-Temperature Phase Transition Behavior and Magnetocaloric Effect in a Sub-Rapidly Solidified La−Fe−Si Plate Produced by Centrifugal Casting. *J. Mater. Sci. Technol.* **2018**, *34* (8), 1337−1343.
(75) Wang, W.; Huang, R.; Li, W.; Tan, J.; Zhao, Y.; Li, S.; Huang, C.; Li, L. Zero Thermal Expansion in NaZn13-Type La(Fe,Si)13 Compounds. *Phys. Chem. Chem. Phys.* **2015**, *17* (4), 2352−2356.
(76) Jun, S.; Yang-Xian, L.; Ji-Rong, S.; Bao-Gen, S. Effect of R Substitution on Magnetic Properties and Magnetocaloric Effects of La1-XRxFe11.5Si1.5 Compounds with R Ce, Pr and Nd. *Chinese Phys. B* **2009**, *18* (5), 2058−2062.
(77) Chen, Y.; Wang, F.; Shen, B.; Hu, F.; Sun, J.; Wang, G.; Cheng, Z. Magnetic Properties and Magnetic Entropy Change of LaFe11.5Si1.5Hy Interstitial Compounds. *J. Phys.: Condens. Matter* **2003**, *15*, L161−L167.
(78) Hu, F. X.; Qian, X. L.; Sun, J. R.; Wang, G. J.; Zhang, X. X.; Cheng, Z. H.; Shen, B. G. Magnetic Entropy Change and Its Temperature Variation in Compounds La(Fe 1-XCo x) 11.2Si 1.8. *J. Appl. Phys.* **2002**, *92* (7), 3620−3623.
(79) Hu, F. X.; Shen, B. G.; Sun, J. R.; Cheng, Z. H.; Rao, G. H.; Zhang, X. X. Influence of Negative Lattice Expansion and Metamagnetic Transition on Magnetic Entropy Change in the Compound LaFe11.4Si1.6. *Appl. Phys. Lett.* **2001**, *78* (23), 3675−3677.
(80) Shen, J.; Li, Y. X.; Dong, Q. Y.; Sun, J. R. Magnetocaloric Properties of the La0.7Pr0.3Fe13-XSix Compounds. *J. Magn. Magn. Mater.* **2009**, *321* (15), 2336−2339.
(81) Wang, F.; Chen, Y. F.; Wang, G. J.; Shen, B. G. The Effect of Mn Substitution in LaFe11.7Si1.3 Compound on the Magnetic Properties and Magnetic Entropy Changes. *J. Phys. D. Appl. Phys.* **2003**, *36* (1), 1−3.
(82) Shen, J.; Gao, B.; Zhang, H. W.; Hu, F. X.; Li, Y. X.; Sun, J. R.; Shen, B. G. Reduction of Hysteresis Loss and Large Magnetic Entropy Change in the Na Zn13 -Type LaPrFeSiC Interstitial Compounds. *Appl. Phys. Lett.* **2007**, *91* (14), 3−5.
(83) Chen, Y. F.; Wang, F.; Shen, B. G.; Sun, J. R.; Wang, G. J.; Hu, F. X.; Cheng, Z. H.; Zhu, T. Effects of Carbon on Magnetic Properties and Magnetic Entropy Change of the LaFe11.5Si1.5 Compound. *J. Appl. Phys.* **2003**, *93*, 6981−6983.
(84) Shen, J.; Gao, B.; Zhang, H. W.; Hu, F. X.; Li, Y. X.; Sun, J. R.; Shen, B. G. Reduction of Hysteresis Loss and Large Magnetic Entropy Change in the Na Zn13 -Type LaPrFeSiC Interstitial Compounds. *Appl. Phys. Lett.* **2007**, *91* (14), 9−12.
(85) Shen, J.; Li, Y. X.; Zhang, J.; Gao, B.; Hu, F. X.; Zhang, H. W.; Chen, Y. Z.; Rong, C. B.; Sun, J. R. Large Magnetic Entropy Change and Low Hysteresis Loss in the Nd- and Co-Doped La (Fe,Si)13 Compounds. *J. Appl. Phys.* **2008**, *103* (7), 1−4.
(86) Hu, F. X.; Ilyn, M.; Tishin, A. M.; Sun, J. R.; Wang, G. J.; Chen, Y. F.; Wang, F.; Cheng, Z. H.; Shen, B. G. Direct Measurements of Magnetocaloric Effect in the First-Order System LaFe11.7Si1.3. *J. Appl. Phys.* **2003**, *93* (9), 5503−5506.
(87) Shen, J.; Wang, F.; Zhao, J. L.; Wu, J. F.; Gong, M. Q.; Hu, F. X.; Li, Y. X.; Sun, J. R.; Shen, B. G. Reduction in Hysteresis Losses and Large Magnetic Entropy Change in the B-Doped La (Fe,Si) 13 Compounds. *J. Appl. Phys.* **2010**, *107* (9), 13−16.
(88) Shen, J.; Gao, B.; Dong, Q. Y.; Li, Y. X.; Hu, F. X.; Sun, J. R.; Shen, B. G. Magnetocaloric Effect in La1-XPrxFe 10.7Co0.8Si1.5 Compounds near Room Temperature. *J. Phys. D. Appl. Phys.* **2008**, *41* (24), 245005.
(89) Lyubina, J. Magnetocaloric Materials for Energy Efficient Cooling. *J. Phys. D. Appl. Phys.* **2017**, *50* (5), 053002.
(90) Feng, S.; Fang, Y.; Zhai, Q.; Luo, Z.; Zheng, H. Magnetocaloric Effect in a Dual-Phase Coupled LaFe11Si2 Crystal Prepared by a Modified High-Pressure Zone-Melting Technique. *J. Cryst. Growth* **2016**, *451*, 83−87.
(91) Imam, H.; Zhang, H. G.; Xu, L.; Zhao, J. L.; Gao, X. X.; Yue, M. The Effects of Tb Substitution for La on the Magnetic Properties of LaFe11.5Si1.5 Compound. *J. Magn. Magn. Mater.* **2018**, *454*, 243−248.
(92) Chen, X.; Chen, Y.; Tang, Y. High-Temperature Phase Transition and Magnetic Property of LaFe 11.6Si1.4 Compound. *J. Alloys Compd.* **2011**, *509* (34), 8534−8541.
(93) Peng, D.R.; Zhong, X.C.; Dong, X.T.; Huang, J.H.; Zhang, H.; Ma, L.; Wu, S.M.; Jiao, D.L.; Liu, Z.W.; Yu, H.Y.; Zhang, H.; Qiu, W.Q.; Ramanujan, R.V. Microstructure, Phase Evolution and Magnetocaloric Properties of LaFe11.6Si1.4/La70Co30 Composite. *J. Alloys Compd.* **2020**, *823*, 153726.
(94) Chen, X.; Chen, Y.; Tang, Y. Influence of Iron on Phase and Magnetic Property of the LaFe 11.6Si1.4 Compound. *J. Rare Earths* **2011**, *29* (4), 354−358.
(95) Zhong, X. C.; Feng, X. L.; Huang, X. W.; Shen, X. Y.; Liu, Z. W. Structure and Magnetocaloric Effect of La0.7Ce0.3(Fe0.92Co0.08)-11.4Si1.6bulk Alloy Prepared by Powder Metallurgy. *J. Alloys Compd.* **2016**, *685*, 913−916.
(96) Lyubina, J.; Gutfleisch, O.; Kuz'min, M. D.; Richter, M. La(Fe,Si)13-Based Magnetic Refrigerants Obtained by Novel Processing Routes. *J. Magn. Magn. Mater.* **2009**, *321* (21), 3571−3577.
(97) Yan, A.; Müller, K. H.; Gutfleisch, O. Structure and Magnetic Entropy Change of Melt-Spun LaFe 11.57Si 1.43 Ribbons. *J. Appl. Phys.* **2005**, *97* (3), 2003−2006.
(98) *Melt spinning*. https://www.mtixtl.com/EQ-VTC-200.aspx (accessed 2023-07-02).
(99) *Box furnace*. https://vbceramics.com/details.php?prod=Box_Furnace_upto_1200%3Csup%3Eo%3C/sup%3EC (accessed 2023-05-03).
(100) Xie, K.; Song, X.; Zhu, Y.; Lv, W.; Sun, Z. Large Magnetic Entropy Change in Melt-Spun LaFe11.5Si 1.5 Ribbons. *J. Phys. D. Appl. Phys.* **2004**, *37* (22), 3063−3066.
(101) Morrison, K.; Lyubina, J.; Moore, J. D.; Caplin, A. D.; Sandeman, K. G.; Gutfleisch, O.; Cohen, L. F. Erratum: Contributions to the Entropy Change in Melt-Spun LaFe 11.6Si 1.4 (Journal of Physics D: Applied Physics (2010) 43 (132001)). *J. Phys. D. Appl. Phys.* **2012**, *45* (17), 179501.
(102) Dai, Y.; Li, Y.; Xu, Z.; Luo, Z.; Han, K.; Zhai, Q.; Zheng, H. Studying of Doping Boron and Carbon in LaFe11.6Si1.4 Magneto-caloric Alloy by Experimental and Density-Functional Methods. *J. Alloys Compd.* **2018**, *765*, 538−543.
(103) Li, L.; Yan, M. Recent Progresses in Exploring the Rare Earth Based Intermetallic Compounds for Cryogenic Magnetic Refriger-ation. *J. Alloys Compd.* **2020**, *823*, No. 153810.
(104) Liu, M.; Yu, B.-f. Development of Magnetocaloric Materials in Room Temperature Magnetic Refrigeration Application in Recent Six Years. *J.Cent.South Univ.Technolo.* **2009**, *16*, 1−12.
(105) Xu, C.; Li, G. D.; Wang, L. G. Itinerant-Electron Metamagnetic Transition and Giant Magnetocaloric Effect in La0.8Ce0.2Fe11.4Si1.6 Compound. *J. Appl. Phys.* **2006**, *99* (12), 10−14.
(106) Chen, X.; Chen, Y.; Tang, Y.; Xiao, D. The System Study of 1:13 Phase Formation, the Magnetic Transition Adjustment, and Magnetocaloric Property in La(Fe,Co)13-XSi x Alloys. *J. Magn. Magn. Mater.* **2014**, *368*, 155−168.
(107) Chen, X.; Chen, Y. G.; Tang, Y. B.; Xiao, D. Q. Effect of Ce, Co, B on Formation of LaCo13-Structure Phase in La(Fe, Si)13 Alloys. *Trans. Nonferrous Met. Soc. China (English Ed.* **2014**, *24* (3), 705−711.
(108) CHEN, X.; CHEN, Y.; TANG, Y. Influence of Iron on Phase and Magnetic Property of the LaFe11.6Si1.4 Compound. *J. Rare Earths* **2011**, *29* (4), 354−358.


https://doi.org/10.1021/acsomega.3c08622
*ACS Omega* 2024, 9, 11110−11128

(109) Blázquez, J. S.; Ipus, J. J.; Moreno-Ramírez, L. M.; Álvarez-Gómez, J. M.; Sánchez-Jiménez, D.; Lozano-Pérez, S.; Franco, V.; Conde, A. Ball Milling as a Way to Produce Magnetic and Magnetocaloric Materials: A Review. *J. Mater. Sci.* **2017**, *52* (20), 11834−11850.
(110) Zhao, F.; Wu, Z.; Huang, Q. Study on the Hydrogenation Kinetics, Properties, and Stability of LaFe11.5Si1.5 and LaFe11.4Si1.6 Compounds. *J. Supercond. Nov. Magn.* **2018**, *31* (2), 505−510.
(111) Pecharsky, A. O.; Gschneidner, K. A.; Pecharsky, V. K. The Giant Magnetocaloric Effect of Optimally Prepared Gd5Si2Ge2. *J. Appl. Phys.* **2003**, *93* (8), 4722−4728.
(112) Xue, J.; Long, Y.; Wang, Y.; Zhou, H.; Zhang, H.; Ye, R. Corrosion Behavior of Nonstoichiometric La(Fe,Si)13-Based Alloys. *J. Phys. Chem. C* **2019**, *123* (47), 28898−28906.
(113) Eggert, B. G. F.; Teixeira, C. S.; Lopes, L. U.; Wendhausen, P. A. P. Feasibility of Nd Substitution in (La, Nd)(Fe, Si)13 Magnetocaloric Compound Obtained by the Reduction-Diffusion Process. *IEEE Trans. Magn.* **2016**, *52* (5), 1−4.
(114) Löwe, K.; Liu, J.; Skokov, K.; Moore, J. D.; Sepehri-Amin, H.; Hono, K.; Katter, M.; Gutfleisch, O. The Effect of the Thermal Decomposition Reaction on the Mechanical and Magnetocaloric Properties of La(Fe,Si,Co) 13. *Acta Mater.* **2012**, *60* (10), 4268−4276.
(115) Hcini, S.; Boudard, M.; Dhahri, A.; Zemni, S.; Bouazizi, M. L. Magnetocaloric Effect Study by Means of Theoretical Models and Spontaneous Magnetization Determination in Ni0.4Mg0.3Cu0.3-Fe2O4 Ferrite. *Mater. Res. Express* **2019**, *6* (6), 066108.
(116) Amaral, J. S.; Amaral, V. S. Simulating the Giant Magnetocaloric Effect-from Mean-Field Theory to Microscopic Models. *Frontiers in Materials*; Frontiers Media: 2023. DOI: 10.3389/fmats.2023.1037396.
(117) Sokolovskiy, V. V.; Miroshkina, O. N.; Buchelnikov, V. D. Review of Modern Theoretical Approaches for Study of Magnetocaloric Materials. *Physics of Metals and Metallography.*; Pleiades Journals: 2022; pp 319−374. DOI: 10.1134/S0031918X22040111.
(118) Huang, J.; Liu, J.; Jin, P.; Yan, H.; Qiu, J.; Xu, L.; Zhang, J. Development of Permanent Magnetic Refrigerator at Room Temperature. *Rare Met.* **2006**, *25* (6), 641−644.
(119) Sari, O.; Balli, M.; Trottet, G.; Bonhote, Ph.; Egolf, P. W. Initial Results of a Test-Bed Magnetic Refrigeration Machine with Practical Running Conditions, *3d Int. Conf. Magn. Refrig. room Temp.* 2009; pp 371−380.
(120) Cheng, J.; Liu, G.; Huang, J.; Liu, C.; Jin, P.; Yan, H. Refrigeration Effect of La(FeCoSi)13B0.25 Compounds and Gadolinium Metal in Reciprocating Magnetic Refrigerator. *J. Rare Earths* **2013**, *31* (12), 1163−1167.
(121) Tušek, J.; Kitanovski, A.; Poredoš, A. Geometrical Optimization of Packed-Bed and Parallel-Plate Active Magnetic Regenerators. *Int. J. Refrig.* **2013**, *36* (5), 1456−1464.
(122) Balli, M.; Sari, O.; Mahmed, C.; Besson, C.; Bonhote, P.; Duc, D.; Forchelet, J. A Pre-Industrial Magnetic Cooling System for Room Temperature Application. *Appl. Energy* **2012**, *98*, 556−561.
(123) Belo, J. H.; Pires, A. L.; Araujo, J. P.; Pereira, A. M. Magnetocaloric Materials : From Micro- to Nanoscale. *J. Mater. Res.* **2019**, *34* (iv), 134.
(124) Lionte, S.; Barcza, A.; Hittinger, M.; Risser, M.; Muller, C.; Katter, M. Recent Experimental Results of First Order LaFeSi-Based Magnetocaloric Materials in an Active Magnetic Regeneration Device. *Refrig. Sci. Technol.* **2018**, 56−61.
(125) Imaizumi, K.; Fujita, A.; Suzuki, A.; Kobashi, M.; Ozaki, K. Novel Approach in Fabricating Microchannel-Structured La(Fe,Si)-13Hy Magnetic Refrigerant via Low-Contamination Route Using Dissolutive Mold. *Mater. Des.* **2022**, *217*, No. 110651.


https://doi.org/10.1021/acsomega.3c08622
*ACS Omega* 2024, 9, 11110−11128